Superresolution architecture of pluripotency guarding adhesions

Aki Stubb[1,#], Camilo Guzmán[1,#], Elisa Närvä[1], Jesse Aaron[2], Teng-Leong Chew[2], Markku Saari[1], Mitro Miihkinen[1], Guillaume Jacquemet[1] and Johanna Ivaska[1,3,*]

1. Turku Centre for Biotechnology, University of Turku, FIN-20520 Turku, Finland
2. Advanced Imaging Center, HHMI Janelia Research Campus, Ashburn, Virginia 20147, USA.
3. Department of Biochemistry and Food Chemistry, University of Turku, Turku FIN- 20520, Finland

# equal contribution

* corresponding author: joivaska@utu.fi

Abstract

Human pluripotent stem cells (hPSC) can generate almost all adult cell lineages. While it is clear that key transcriptional programmes are important elements for maintaining pluripotency, the equally essential requirement for cell adhesion to specific extracellular matrix components remains poorly defined. Our recent observation that hPSC colonies form unusually large “cornerstone” focal adhesions (FA), distinct from parental somatic cells, that are lost following differentiation, emphasises the potential of these atypical FA as gatekeepers of pluripotency. Here, using nanopatterns, we further demonstrate that physical restriction of adhesion size, in hPSC colonies, is sufficient to trigger differentiation. Using superresolution two-colour interferometric photo-activated localization microscopy (iPALM), we examined the three-dimensional architecture of these cornerstone adhesions and report vertical lamination of FA proteins with three main structural peculiarities: 1) integrin β5 and talin are present at high density, at the edges of cornerstone FA, adjacent to a vertical kank-rich protein wall. 2) Vinculin localises higher than expected with respect to the substrata, and 3) surprisingly, actin and α-actinin are present in two discrete layers, a previously undescribed localisation for these proteins. Finally, we report that depletion of kanks diminishes FA patterning, and actin organisation within the colony, indicating a key role for kanks in hPSC colony architecture.

Introduction

Human Pluripotent Stem Cells (hPSC) have the capacity to self-replicate and to differentiate into virtually any cell type of the human body. Therefore they have great therapeutic potential. hPSC can be generated by artificially reprogramming somatic cells (Takahashi et al., 2007; Yu et al., 2007) and studies have focused on how transcriptional programs control pluripotency as well as on the development of protocols to induce specific differentiation programs (Boyer et al., 2005). To ensure the safe use of hPSC in a clinical setting, hPSC need to be maintained in animal serum- and feeder layer-free culture conditions that allow hPSC to remain pluripotent. Importantly, hPSC remain pluripotent, in vitro, in 2D cultures, when they adhere to specific extracellular matrix (ECM) molecules (Braam et al., 2008; Rodin et al., 2014; Baxter et al., 2009), highlighting a fundamental role for the ECM as well as their receptors for stemness.

Cells interact with the surrounding ECM via transmembrane adhesion receptors, such as integrins, which provide a physical link between the ECM and the actin cytoskeleton (Askari et al., 2009). Integrin engagement leads to the assembly of large signalling platforms termed focal adhesions (FA), which modulate most cellular functions (Legate et al., 2009). FAs are highly dynamic and complex structures composed of hundreds of proteins (Horton et al., 2015) that tune cellular responses, but their overall architecture can be studied using an handful of key adaptors. Indeed, advances in superresolution light microscopy have enabled the determination of the precise nanoscale architecture of FAs in cancer cells. Previous studies have demonstrated highly organized vertical stratification of FAs using iPALM (Kanchanawong et al., 2010; Liu et al., 2015; Case et al., 2015), a technique that combines interferometry and photoactivated localization microscopy (PALM) to provide sub 20-nm, three-dimensional isotropic (3D) localization of tagged proteins (Shtengel et al., 2009). FA proteins localize to three general functional layers: a membrane proximal integrin signalling layer (composed of integrins, paxillin and focal adhesion kinase), an intermediate force transduction layer (composed of talin and vinculin) and an actin regulatory layer (composed of both actin and actin regulatory elements) (Kanchanawong et al., 2010; Liu et al., 2015; Case et al., 2015). Interestingly, vinculin a binding partner for many FA proteins and a key stabilizer of talin unfolding has been shown to display a wide distribution across all three layers with increasing upward positioning in mature FAs (Case et al., 2015).

Even though integrins, have been implicated as key requirements for the maintenance of pluripotency in vitro (Rodin et al., 2014; Braam et al., 2008; Meng et al., 2010), much less is known about the focal adhesion composition and organisation of hPSC. Previously we described that the

hallmark sharp hPSC colony edge is regulated by unusually large FA, termed cornerstone adhesion, that are connected by strong contractile ventral stress fibres termed actin “fence” (Närvä et al., 2017). Furthermore, these colony edge adhesions exert strong traction-forces on the underlying ECM which regulates colony morphology and the orientation of hPSCs cell divisions (Närvä et al., 2017).

Here we have used nano-grated patterns to investigate the link between FA morphology and pluripotency and a combination of high- and superresolution microscopy techniques including, iPALM, structure illumination microscopy (SIM) and Airyscan to determine the three-dimensional architecture of cornerstone FAs present at the periphery of hPSC colonies. We find that mere physical restriction of FA size and orientation in hPSC colonies is sufficient to compromise expression of SOX2 and SSEA-1, indicating a key role cornerstone FA architecture as “guarding” pluripotency. In addition, we find that the nanoscale localization of several of the key FA components: integrins αV and β5, paxillin, vinculin, talin, actin and α-actinin, proteins previously mapped in classical FA (Kanchanawong et al., 2010), is markedly distinct in hPSC FAs. Furthermore, we have included novel FA scaffold partners kank1 and kank2 in our imaging and describe a key role for Kanks in regulating hPSC adhesion and maintaining FA architecture in pluripotent cells.

Results

hPSC cornerstone FA architecture is essential for maintaining pluripotency

hPSC colonies plated on vitronectin (VTN), an ECM ligand which supports pluripotency (Braam et al., 2008), assemble into tightly packed colonies with well-defined edges (Thomson et al., 1998). Structurally, these colonies are encircled by unusually large paxillin-positive FA termed “cornerstone” FAs that are themselves connected by prominent actin bundles termed “actin fence” (Fig. 1a and Supplementary Fig. 1a, (Närvä et al., 2017)). Live cell imaging of endogenously-tagged paxillin revealed that hPSC cornerstone FAs are remarkably stable compared to the FA formed at the centre of hPSC colonies (Supplementary Fig. 1b, video 1). Structured illumination microscopy imaging of cornerstone FA revealed that they can be composed of multiple linear units clustered together (Supplementary Fig. 1c).

The unique properties of cornerstone FA (size, orientation and stability), led us to speculate that they are key regulators of colony morphology and could contribute to pluripotency maintenance. To constrain the orientation and the maximal size of FA, hPSC colonies were plated on VTN-coated nano-grated pattern composed of alternating 800 nm wide matrix ridges and 600 nm deep grooves (Fig. 1b and 1c). These nanopatterns were sufficient to constrict FA size as the characteristic area of FAs found on uniform surfaces is 4.2 μm^2 while when plated on nanopatterns the characteristic FA area was reduced to 1.8 μm^2. Remarkably, when plated on nanopatterns (Fig. 1b and 1c), characteristic rounded morphology, actin fence and cornerstone FA of the hPSC colonies were distorted (Fig. 1a and 1b). To allow cells to follow spontaneous differentiation, cells can be exposed to E6 media without bFGF and TGFβ. Three day exposure to VTN-coated nanopattern surface in E6 media was sufficient to decrease the level of the pluripotency factor Sox2 while increasing the level of differentiation marker SSEA-1 (Fig. 1d, 1e and 1f). In contrast, cells maintained in E6 media on uniform VTN-coated surface remained Sox2 positive and SSEA-1 low (Fig. 1d, 1e and 1f). Strikingly, the efficacy of the nano-pattern induced differentiation was comparable to BMP-4 treatment, on uniform surface, which was used as a positive control for differentiation (Fig. 1e and 1f). These data clearly demonstrate that physical constrain of FA size and orientation in hPSC colonies is alone sufficient to compromise pluripotency and induce differentiation. Importantly these data indicate a critical role for cornerstone FA architecture in guarding pluripotency and prompted us to investigate their nanoscale architecture in more detail.

iPALM imaging of hPSC cornerstone focal adhesions

To investigate the ultrastructure of hPSC cornerstone FA, we used interferometric photo-activated localization microscopy (iPALM), a strategy that provides sub 20-nm 3D localization of molecules (Shtengel et al., 2009). iPALM imaging of core FA proteins previously revealed that FAs in osteosarcoma cells (U2OS) display a well-organized architecture composed of at least three distinct, vertically separated, functional layers (integrin signalling layer, force transduction layer and actin regulatory layer) (Kanchanawong et al., 2010). To assess the organisation of these layers in hPSC cornerstone FAs, representative proteins localising to each layer were chosen to be imaged. For the integrin signalling layer, proteins chosen include the vitronectin binding integrins αV and β5 as well as paxillin. Talin-1 and vinculin were chosen as core components of the force transduction layer and α-actinin-1 and actin for the actin regulatory layer (Kanchanawong et al., 2010). In addition, both kank1 and kank2, two recently described FA proteins, were included due to their unique localisation at the outer-rim of FA (Sun et al., 2016; Bouchet et al., 2016). The long-isoform of kank1 (Bouchet et al., 2016) is highly expressed in the hPSC (Supplementary Fig. 2), and therefore this isoform was chosen.

Efficient iPALM requires the use of photo-switchable labels as well as high density labelling (Shtengel et al., 2009) which render the imaging of endogenous molecules difficult. Therefore and as previously done by others for iPALM (Kanchanawong et al., 2010; Case et al., 2015; Liu et al., 2015), FA proteins of interest tagged with the photoactivatable fluorescent protein (PA-FP) mEOS were transiently expressed in hPSC. In addition, to image the FA proximal kank1 and kank2 proteins using iPALM, mEOS -tagged constructs were generated (see methods for details). Importantly, the proteins chosen are endogenously expressed in hPSC (Supplementary Fig. 2) and localise to cornerstone FA (imaging of endogenous proteins; Supplementary Fig. 3). Furthermore we validated that the transiently expressed constructs used for iPALM localized properly and did not affect colony morphology or the protein level of the pluripotency marker OCT4 (Supplementary Fig. 4).

Talin-1 and integrin β5 accumulate at the periphery of large cornerstone adhesions.

Using iPALM, we first determined the lateral distribution of the FA proteins localising to the various functional layers. All proteins, with the exception of β5 integrin and talin-1, displayed homogeneous x-y distribution and density within cornerstone FA. On the other hand, β5 integrin and talin-1 revealed an obvious ring-like distribution with more proteins localizing to the edges of the largest cornerstone adhesion (Fig. 2a-c). Integrin αV can dimerize, not only with β5 integrin, but

also with multiple other β-subunits (Humphries et al., 2006), which may explain why integrin αV is homogeneously distributed throughout the cornerstone adhesion.

To assess the endogenous distribution of integrin β5 and talin, within cornerstone FA, hPSC were stained and imaged using an Airyscan confocal microscope. As observed with iPALM, endogenous talin also accumulated at the edges of large cornerstone adhesion (Supplementary Fig. 5a and 5b). Interestingly, in most cornerstone adhesions endogenous β5-integrin as well as αVβ5-integrins were strongly distributed to FA edges (Fig. 2d and Supplementary Fig.5c) while active β1-integrin or paxillin distributed uniformly throughout the interior of the adhesion (Fig. 2d and Supplementary Fig.5d). Thus, in hPSC the integrin signalling layer is horizontally segregated in subregions of different vitronectin binding integrins.

Talin is fully extended throughout the cornerstone focal adhesions

We next used iPALM to determine the vertical positioning of the adhesion proteins imaged (the distance from the coverslip is measured) (Fig. 2e). The components of the integrin signalling layer (integrin β5, integrin αV and paxillin) have a Z-positioning indicating a close relationship with the cell membrane and their vertical distribution values are very similar to those reported for U2OS FA (Fig. 2f). However, the Z-positioning of talin-1 and vinculin, components of the force transduction layer (Fig. 3a), were found to be higher than previously reported for U2OS FAs (Kanchanawong et al., 2010; Liu et al., 2015; Case et al., 2015) (Fig. 3b and 3c).

Talin can adopt multiple conformations in the cell, ranging from a head to tail auto-inhibited conformation to a fully extended, integrin and actin bound mechanically stretched conformation (Yao et al., 2016). To evaluate the 3D FA distribution of talin as well as its vertical extension, we imaged both N-terminally (talin-N) and C-terminally (talin-C) tagged talin-1 (Liu et al., 2015; Bouissou et al., 2017). Overall, the Z-position values for talin-N ($Z_{centre} = 72.8 \pm 12.3\, nm$) and for talin-C ($Z_{centre} = 103.5 \pm 20.5\, nm$) are higher than those reported for U2OS cells (Liu et al., 2015). However, the distance between the two ends of talin were comparable to the distance previously measured. This has been considered to represent the extended talin conformation (Case et al., 2015; Liu et al., 2015; Bouissou et al., 2017). Calculations of the inclination angle based on the vertical separation of the two ends and the full length of the protein, indicated an approximated value of $\theta \approx 17°$ which is also in agreement with previous work (Liu et al., 2015). Thus, our results indicate that talin is fully extended throughout the adhesion and that, in large FAs, talin clusters at higher density at the edges of the adhesions (Fig. 2c).

Vinculin displays a head above the tail orientation and a cup-like shape distribution.

In classical FA, vinculin displays a wide vertical distribution and has a preferred orientation with the tail above the head (Case et al., 2015). iPALM analyses of N-terminally (vinculin-N) and C-terminally (vinculin-C) tagged vinculin constructs (Fig. 3c and Supplementary Fig. 6a) revealed that vinculin vertical positioning in hPSC cornerstone adhesion is significantly higher than in classical FA (Kanchanawong et al., 2010; Case et al., 2015). Increase in vinculin Z positioning has been linked to vinculin activation and focal adhesion maturation (Case et al., 2015), suggesting that hPSC cornerstone adhesions are mature and contain active vinculin. Very unexpectedly, vinculin was oriented "head above the tail" in hPSC cornerstone adhesions (vinculin-N, $Z_{centre} = 100.4 \pm 14.4\,nm$; vinculin-C, $Z_{centre} = 76.4 \pm 16.3\,nm$) (Fig. 3c). Using a two-colour iPALM strategy, where both endogenous paxillin and vinculin-C could be imaged at high resolution in the same cells, we were able to validate that vinculin tail is indeed in close relationship with the integrin signalling layer (Fig. 3d). This "head above the tail" vinculin conformation could be indicative of an extreme activation state of vinculin that may be triggered by the high forces exerted in cornerstone FA (Närvä et al., 2017). Indeed, vinculin has been reported to dissociates from talin in cases where forces borne by an individual protein exceed 25 pN (Yao et al., 2014). In such cases, it is possible that the vinculin head will bind a different partner that localises higher up in cornerstone FA (such as α-actinin-1) or that the vinculin tail engages components close to the plasma membrane such as paxillin or PI(4,5)P_2 (Carisey and Ballestrem, 2011).

In addition to an inverted orientation, 3D rendering of the acquired localisations for vinculin revealed that its distribution is not homogeneously flat within cornerstone FA but rather that its distribution forms a solid paraboloid or "cup-like" shape (Fig. 3e). We could confirm that this cup-like shape is specific to vinculin as it could not be observed for paxillin (Fig. 3e). This distribution means that more membrane distal vinculin molecules occupy a larger lateral area than the membrane proximal vinculin (Fig. 3f). The spatially controlled intra-FA z-distribution of vinculin (Fig. 3e) as well as the ring shaped distribution of talin and β5 integrin (Fig. 2) suggest that the edge of the pluripotency FAs is architecturally unique from the centre.

The unexpected three-dimensional orientation of vinculin in the cornerstone FAs prompted us to investigate the role of vinculin in hPSC colony morphology and pluripotency maintenance. We used lentivirus shRNA to silence 95% of endogenous vinculin (Supplementary Fig. 6b). Imaging of VTN plated control and shvinculin hPSC colonies showed that vinculin silencing neither disrupted colony formation, actin fence formation or cornerstone FA (Supplementary Fig. 6c and 6d). Vinculin

silencing appeared to only modestly increase the size of the FA found at the centre of hPSC colonies. In addition, silencing of vinculin did not affect the expression level of Oct4 (Supplementary Fig. 6b) indicating that vinculin is not needed for the maintenance of pluripotency in these conditions.

Cornerstone adhesions have two vertically separated actin layers

Cornerstone FAs are connected by prominent ventral actin bundles (Fig. 1 and Supplementary Fig. 1) and therefore actin is found both inside and outside FA. To accurately determine the vertical positioning of actin within cornerstone FA, endogenous paxillin was used as a reference marker and two-colour iPALM was performed (Fig. 4a and 4b). Unlike the proteins in the integrin signalling and the force transduction layers, actin distribution within cornerstone FA was not gaussian but could instead be described as the sum of two Gaussian distributions (Fig. 4c). This indicates that, much to our surprise, and in contrast to conventional FA nanoscale architecture (Kanchanawong et al., 2010), actin forms two coexisting vertical layers separated, by a ~50 nm gap on top of the cornerstone FA (Fig. 4b and 4c).

This axial actin localization pattern was further confirmed by the distribution of α-actinin-1, a protein typically overlapping with actin (Carisey et al., 2013). α-actinin-1 also presented the same two-peak distribution than actin albeit with a slight shift in Z positioning (Fig. 4d and 4e). Importantly, the separation between the two actin peaks and the two α-actinin-1 peaks is identical suggesting that each actin peak has an associated α-actinin-1 peak. The vertical position of the first actin ($Z_{centre} = 99.6 \pm 14.4\, nm$) and α-actinin-1 ($Z_{centre} = 125.5 \pm 15.1\, nm$) peaks matches the Z-position reported for these proteins in U2OS cells (Kanchanawong et al., 2010). In contrast, the second peak for actin ($Z_{centre} = 155.4 \pm 14.2\, nm$) and α-actinin-1 ($Z_{centre} = 174.8 \pm 17.1\, nm$) represents a previously undescribed higher localising actin population (Fig. 4f). In the future, it will be interesting to determine how this is regulated and which proteins occupy the unique ~50 nm gap between the two vertically separated actin layers.

Nanoscale localization of focal adhesion scaffold proteins kank-1 and kank-2

Having established that pluripotency FAs display three-dimensional stratification of integrin signalling, force transduction and actin stress fiber layers, albeit with substantial deviation from the ones described previously (Liu et al., 2015; Case et al., 2015; Kanchanawong et al., 2010) and clear distinction between FA edge and centre, we proceeded to search for possible scaffold proteins that

could uniquely regulate FA edges. Two recent reports have described that evolutionary conserved scaffold proteins kank1 and kank2 localise to the border of focal adhesions linking them to talin and the actin cytoskeleton (Sun et al., 2016; Bouchet et al., 2016).

We performed two-colour iPALM of kank1 and kank2 together with endogenous paxillin to enable precise determination of kank 3D localization with respect to FA (Fig. 5a-d). kank1 localised predominantly at the border of paxillin -positive FAs with individual molecules detected also inside adhesions (Fig. 5a). This localisation was validated with endogenous staining and high-resolution Airyscan imaging of kank1 (Supplementary Fig. 3). In contrast, kank2 was always observed at the outer-rim or outside paxillin -positive FAs in hPSC (Fig. 5c). In addition, kank2 only accumulated near very large cornerstone FA, always towards their distal end, and occasionally following the direction of ventral stress fibres (Fig. 5c). Vertically both kank1 and kank2 localisation varied depending on their proximity to FAs. At the outer-rim of FAs, both kank1 and kank2 displayed higher Z-positions than paxillin (60 nm above paxillin) that correspond to the height of the force transduction layer (Video 2, Fig. 5a). Interestingly, in paxillin-negative structures, both kank1 and kank2 localised at a lower vertical position indicating a close proximity to the plasma membrane (Fig. 5b and 5c). The Z-positions obtained for kank1 and kank2 adjacent to FA were ($Z_{centre} = 116.1 \pm 12.1\, nm$) and ($Z_{centre} = 100.8 \pm 13.4\, nm$), respectively. kank1 and kank2 distant from FA localised respectively at Z-positions ($Z_{centre} = 63.4 \pm 13.6\, nm$) and ($Z_{centre} = 74.2 \pm 17.7\, nm$) (Fig. 5e).

Kank proteins modulate adhesion size and properties in somatic cells by both regulating integrin function and microtubule targetting (Rafiq et al., 2018). As both kank1 and kank2 localise at the outer-rim of hPSC cornerstone adhesions, we wanted to investigate the contribution of kank1 and kank2 to cornerstone adhesion properties. Unexpectedly, down-regulation of kank1 and kank2 expression using siRNA led to smaller cornerstone FAs at the colony edge while the FA located at the centre of hPSC colonies centre became larger (Fig. 5e, 5f and Supplementary Fig. 7). Thus, kank1 and kank2 are important regulators of the intra-colony distinction of colony centre and edge cells and very interestingly differentially regulates the dynamics of the large cornerstone FAs and the smaller adhesions in the colony centre.

Discussion

Pluripotency of human stem cells (hPSC) can be maintained in vitro only when hPSC adhere to specific extracellular matrix molecules such as vitronectin (Braam et al., 2008), highlighting the fundamental role of the adhesion machinery in promoting stemness. We recently described that hPSC colonies are encircled by a strong contractile actin fence connected by exceptionally large focal adhesions (FA) termed cornerstone FA (Närvä et al., 2017). These adhesions are aligned to the colony edge and exert high traction forces upon the substrate (Närvä et al., 2017). Here, we investigated the role of these cornerstone adhesions in regulating pluripotency as well as studied their 3D architecture using super-resolution microscopy.

Detailed analyses of cornerstone adhesions using multiple microscopy approaches revealed that they possess unique properties. Live cell imaging of endogenously-tagged paxillin revealed that they are remarkably stable compared to the FA formed at the centre of hPSC colonies. In addition, their size and orientation were essential for pluripotency since restricting the maximal size and the orientation of cornerstone FAs using nanopatterning was sufficient to alter colony morphology and trigger differentiation. These results demonstrate that cornerstone FAs are guardians of pluripotency in vitro and indicate that their overall architecture is key to their function.

Super resolution iPALM imaging of core FA proteins revealed that cornerstone FA display a well-organized architecture composed of distinct, vertically demarcated, functional layers (Fig. 6a and 6b). Congruent with classical focal adhesion (Kanchanawong et al., 2010), these layers include a membrane proximal integrin signalling layer composed of integrins and paxillin and a force transduction layer composed of talin and vinculin. The components of the integrin signalling layer (integrin β5, integrin αV and paxillin) have a Z-positioning indicating a close relationship with the cell membrane and their vertical distribution values are very similar to those reported for U2OS FA (Fig. 6a) (Kanchanawong et al., 2010; Liu et al., 2015; Case et al., 2015). However, the Z-positioning of talin-1 and vinculin, components of the force transduction layer, were found to be higher than previously reported for U2OS FAs (Kanchanawong et al., 2010) (Fig. 6a). Unlike classical FAs, cornerstone FA feature an unprecedented bi-phasic actin regulatory layer (defined by actin and α-actinin-1) where two discrete vertical actin layers are separated by less actin dense 50 nm gap. This gap may constitute a functional layer in its own right and future work will aim at identifying which proteins localise there. In addition, it will be interesting to determine how these two actin layers are regulated and structurally organised.

Here, we also determined for the first time the 3D organization of kank1 and kank2 with respect to the core adhesion. As previously reported for classical FA (Sun et al., 2016; Bouchet et al., 2016),

both kank1 and kank2 were laterally distributed around cornerstone FA. 3D localisations of kank1 and kank2 revealed that they assemble strong FA-edge defining vertically extended “walls” at the outer-rim of the paxillin positive FAs rather than a belt. The vertical positioning of kanks around FAs indicate that they are in close proximity to the force transduction layer, which is consistent with the ability of kanks to bind to talin (Bouchet et al., 2016). However, further away from the adhesions both kank1 and kank2 localised vertically much lower, suggesting that recruitment of kanks to FA edges is distinct to their assembly to long protein assemblies outside of FAs. Functionally, kanks regulate the colony centre small focal adhesions distinctly from the colony edge FAs. Kank silencing induced larger and more prominent FAs in the colony centre which is in line with previous work suggesting that in fibroblasts kank2 functions to limit integrin activity and facilitate adhesion sliding (Sun et al., 2016). Why the opposite is true for the corner stone FAs at the colony edge is intriguing and remains to be investigated.

Detailed imaging also revealed a lateral segregation of specific proteins within the largest cornerstone adhesions. In particular, β5-integrin was found to assemble high-density ring-like clustering at the edges of adhesions while β1 or αV-integrins were found to be more homogeneously distributed. Within classical focal adhesion, distinct integrin heterodimers display different dynamics (Rossier et al., 2012) or cluster differently depending on their activation states (Spiess et al., 2018). However, the spatial segregation of specific integrin heterodimers appears to be a unique feature of cornerstone adhesions. This interesting centre-edge segregation within cornerstone FA was observed with some of the FA components. Talin density was highest at the FA edges and the vertical distribution of vinculin was higher at FA edges compared to the centre. This apparent intra-FA organisation could be linked to the exceptionally large size of the cornerstone FA and specific interactions of FA components with proteins localising to outer rim of the FAs (FA belt) such as kanks (Bouchet et al., 2016; Sun et al., 2016). All together these data indicate that the edges of cornerstone adhesions are structurally distinct from the centre and it is tempting to speculate that that the edge and the center may serve different biological functions.

Materials and methods

Reagents, antibodies and compounds

Mouse primary antibodies used in this study were against paxillin (BD biosciences, 612405, 1:1000 for western blotting (WB), 1:100 for immunofluorescence (IF)), β-actin (Sigma Aldrich, Clone AC-15, Cat. No. A1978), gapdh (Hytest, 5G4MaB6C5, 1:5000 for WB), Sox2 (R&D systems, MAB2018, 1:1000 for WB), vinculin (Sigma aldrich, V9131, 1:1000 for WB, 1:100 for IF), talin (Sigma Aldrich, clone 8D4 ,T3287, 1:1000 for WB, 1:100 for IF), β1 integrin (clone 12G10, in-house production), α-actinin (Sigma aldrich, A5044, 1:100 for IF). Rabbit primary antibodies used in this study were against oct3/4 (Santa Cruz, sc-9081, 1:1000 for WB, 1:100 for IF), kank1 (Bethyl, A301-882A, 1:1000 for WB, 1:100 for IF), kank2 (Sigma aldrich , HPA015643, 1:1000 for WB), integrin β5 (Cell Signaling Technology, 3629, 1:100 for IF), paxillin (Santa Cruz, sc-5574, 1:100 for IF and for IPALM). The goat anti-Nanog antibody was from R&D systems (AF1997, 1:100 for IF). The secondary antibodies used in this study were all from Thermo Fischer Scientific and used at 1:300. These antibodies included Alexa Fluor 488 donkey anti-rabbit IgG, Alexa Fluor 488 donkey anti-mouse IgG, Alexa Fluor 568 donkey anti-rabbit IgG, Alexa Fluor 568 donkey anti-mouse IgG, Alexa Fluor 647 donkey anti-goatIgG and Alexa Fluor 647 goat anti-mouse IgG. SiR-actin was provided by Cytoskeleton (Cat. No. CY-SC001). Atto 405 Phalloidin and Alexa Fluor 488 phalloidin were provided by Thermo Fisher Scientific.

Plasmids

The following plasmids were provided by Addgene (gift from, Addgene plasmid number): tdEos-Talin-18 (Michael Davidson, 57672) (Kanchanawong et al., 2010), tdEos-Talin-N-22 (Michael Davidson, 57673) (Kanchanawong et al., 2010), tdEos-Vinculin-14 (Michael Davidson, 57691) (Kanchanawong et al., 2010), mEos2-Vinculin-N-21 (Michael Davidson, 57439), tdEos-Lifeact-7 (Michael Davidson, 54527) (Kanchanawong et al., 2010), mEos2-Actin-7 (Michael Davidson, 57339) (Kanchanawong et al., 2010), mEos2-Alpha-Actinin-19 (Michael Davidson, 57346) (Kanchanawong et al., 2010), tdEos-Paxillin-22 (Michael Davidson, 57653) (REF), pSpCas9(BB)-2A-GFP (Feng Zhang, 48138) (Ran et al., 2013), AICSDP-1:PXN-EGFP (The Allen Institute for Cell Science, 87420) (Roberts et al., 2017).

The plasmid encoding β5-integrin-mEOS2 was a kind gift from Martin Humphries (University of Manchester, UK). GFP-kank1 and GFP-kank2 plasmids were gifts from Reinhard Fässler (Max Planck Institute of Biochemistry, Martinsried, DE) (Sun et al., 2016).

Cell culture, gene silencing and transient transfection

hPSC line HEL24.3 was obtained from the University of Helsinki. Cell lines were created using Sendai viruses (Mikkola et al., 2013; Trokovic et al., 2015). Cells were grown in feeder-free conditions on Matrigel (MG) (Corning, 354277) or 5 µg/ml vitronectin (VTN) (Life Technologies, A14700) in Essential 8 (E8) Basal medium (Life Technologies, A15169-01) supplemented with Essential 8 supplement (Life Technologies, A1517-01) at +37°C, 5 % CO_2 in a humidified incubator. Culture media was changed daily. For passaging, cells were detached using sterile filtered 0.5 mM EDTA (Life Technologies, 15575-038) in PBS for 3 min at room temperature (RT). The parental fibroblast cell line of HEL24.3 was obtained from the University of Helsinki, and were cultured in Dulbecco's Modified Eagle's Medium: Nutrient Mixture F-12 (DMEM/F-12) (Life Technologies, 10565-018) supplemented with 10 % Fetal Bovine Serum (FCS) (Biowest, S1860) at +37°C, 5 % CO_2 in a humidified incubator. Fibroblasts were passaged using 0.25% trypsin-EDTA in HBSS (Biowest, L0931-100). U2OS osteosarcoma cells were grown in DMEM supplemented with 10% FCS. U2OS cells were purchased from DSMZ (Leibniz Institute DSMZ-German Collection of Microorganisms and Cell Cultures, Braunschweig DE, ACC 785).

To induce hiPSCs differentiation, cells were cultured on VTN-coated plates and subsequently differentiated using mixture of E6 media and 100 ng/ml BMP-4 (R&D systems, 314-BP). The differentiation media was changed daily and the samples were collected after 72 h.

Plasmids of interest were transfected using DNA-in reagent (MTI-Global Stem) according to the manufacturer instructions. Briefly, 24 h before transfection the cells were seeded on MG to obtain correct confluency. DNA-in reagent and plasmid DNA was mixed in ratio of 1:3 (µg of DNA : µl of regent) to Opti-MEM reduced serum media 15 min before the transfection. Cells were gently detached using 0.5 mM EDTA in PBS and diluted to E8 and mixed with Opti-MEM. Cells were gently pipetted up and down to ensure proper entrainment. Mixture were then added to VTN coated glass and incubated for 20-24 h in culture conditions.

To transiently suppress kank1 and kank2 expression in hiPSCs, Accell siRNA pools (Dharmacon, kank1 E-012879-00-0005; kank2 E-027345-00-0005) were used according to the manufacturer's protocol. siRNA were diluted at a final concentration of 1 µM. siRNA transfection was done first in suspension during the cell passage and repeated after 24h on adherent cells. 48h after the initial transfection cells were plated on VTN coated plates and grown 24h before the fixation or protein

sample collection. siRNAs used as a control were Accell Non-targeting Pool (Dharmacon, D-001910-10-20).

To stably suppress vinculin expression in hIPSCs, cells were transduced with shRNA containing viral particles in suspension during the cell passage. Puromycin selection (2 µg/ml) was started 48 h after the transduction. The shRNA used as control (shCTRL) was shScramble provided by Sigma aldrich (SHC002, sequence: CCG GCA ACA AGA TGA AGA GCA CCA ACT CGA GTT GGT GCT CTT CAT CTT GTT GTT TTT). The shRNAs targeting vinculin shVin#1 (TRCN0000116755, sequence : CCG GCG GTT GGT ACT GCT AAT AAA TCT CGA GAT TTA TTA GCA GTA CCA ACC GTT TTT G) and shVin#2 (TRCN0000116756, sequence: CCG GGC TCG AGA TTA TCT AAT TGA TCT CGA GAT CAA TTA GAT AAT CTC GAG CTT TTT G) were provided by the functional genomics unit of the University of Helsinki.

Generation of C-terminally tagged kank1 and kank2 tdEos constructs

XhoI/EcoRI restriction sites were introduced to flank both mouse kank1 and kank2 genes using polymerase chain reaction (PCR) (Phusion hot start II polymerase, Thermo Scientific). Primers used were kank1_For (5'-AAT ACT CGA GAT GGC TTA TAC CAC AAA AGT TAA TG-3') kank1_Rev (5'-AAT AGA ATT CCG TCA AAA GAA CCT CGG TGA G-3'), kank2_For (5'-AAT ACT CGA GAT GGC CCA GGT CCT GC-3') and kank2_Rev (5'-AAT AGA ATT CCC TCC TCG GCT GAA GAC GA-3'). Following PCR amplification, kank1 and kank2 sequences were inserted into tdEos backbone using XhoI/EcoRI restriction sites. The constructs were sequenced to validate integrity.

Generation Paxillin-GFP Cell Line

The endogenously tagged paxillin hPSC line was generated as previously described (Roberts et al., 2017). Briefly, the gRNA sequence targeting paxillin (5'-GCACCTAGCAGAAGAGCTTG-3') was introduced into pSpCas9(BB)-2A-GFP backbone using the BbsI restriction site. The template plasmid (AICSDP-1:PXN-EGFP) was provided by Addgene (Roberts et al., 2017). HEL 24.3 hPSC cell line was transfected with the GFP-Cas9-paxillin_gRNA construct and template plasmid (AICSDP-1:PXN-EGFP) in equimolar ratio (1:1). After transfection the cell line was cultured for 5 days before sorting the cells based on green fluorescence with FACS.

Nanopattern experiments

HiPSCs were seeded to Nanopattern surface topography dishes (Nanosurface Biomedical) coated with 5 µg/ml VTN-N. Width of individual Nanosurface topography was 800 nm and depth 600 nm covering the glass parallel to each other. Cells were cultured on nanopatterns 24 h for microscopy or 3 days for protein analysis using E6 medium at identical conditions to previously described. Samples were then acquired ether fixing the cells with 4% PFA in PBS for microscopy or lysing the cells to TXLB buffer for protein analysis.

SDS–PAGE and quantitative western blotting

Protein extracts were separated under denaturing conditions by SDS–PAGE and transferred to nitrocellulose membranes. Membranes were blocked for 1 h at room temperature with blocking buffer (LI-COR Biosciences) and then incubated overnight at 4 °C with the appropriate primary antibody diluted in blocking buffer. Membranes were washed with PBS and then incubated with the appropriate fluorophore-conjugated secondary antibody diluted 1:5,000 in blocking buffer for 2 h. Membranes were washed in the dark and then scanned using an Odyssey infrared imaging system (LI-COR Biosciences). Band intensity was determined by digital densitometric analysis using Odyssey software.

Immunofluorescence

Cells were seeded on VTN coated microscopy dishes for 20-24 h. Before fixation cells were washed twice with PBS. Fixation and permeabilization was done simultaneously using 4% PFA and 0.3% Triton-X-100 in PBS for 15 min and washed with PBS. Samples were then quenched with 0.1 M Glycine for 10 min and washed with PBS. The primary antibodies were diluted to 1% BSA in PBS and incubated either 2 h in RT or +4°C overnight. The samples were washed twice with PBS and secondary antibodies diluted into 1% BSA in PBS added for 2 h RT. Sample were then washed with 0.2% Tween 20 in for 10 min in RT followed by PBS wash.

Microscopy

The confocal microscope used was a laser scanning confocal microscope LSM880 (Zeiss) equipped with an Airyscan detector (Carl Zeiss). Objectives used were 40x water (NA 1.2) and 63× oil (NA 1.4). The microscope was controlled using Zen Black (2.3) and the Airyscan was used in standard super-resolution mode.

The SDC microscope used was a Marianas spinning disk imaging system with a Yokogawa CSU-W1 scanning unit on an inverted Zeiss Axio Observer Z1 microscope controlled by SlideBook 6 (Intelligent Imaging Innovations, Inc.). Objectives used were a 20× (NA 0.8 air, Plan Apochromat, DIC) objective (Zeiss), a 63× oil (NA 1.4 oil, Plan-Apochromat, M27 with DIC III Prism) objective (Zeiss), or a 100× (NA 1.4 oil, Plan-Apochromat, M27) objective. Images were acquired using an Orca Flash 4 sCMOS camera (chip size 2,048 × 2,048; Hamamatsu Photonics).

The structured illumination microscope (SIM) used was DeltaVision OMX v4 (GE Healthcare Life Sciences) fitted with a 60× Plan-Apochromat objective lens, 1.42 NA (immersion oil RI of 1.514) used in SIM illumination mode (five phases × three rotations). Emitted light was collected on a front illuminated pco.edge sCMOS (pixel size 6.5 µm, readout speed 95 MHz; PCO AG) controlled by SoftWorx.

The total internal reflection fluorescence (TIRF) microscope used was a Zeiss Laser-TIRF 3 Imaging System equipped with a 63× (1.46 oil objective, α Plan-Apochromat, DIC) objective. Images were acquired on an EMCCD camera (ImageEM C9100-13; chip size 512 ×512; Hamamatsu Photonics) controlled by Zen software (Zen 2012 Blue Edition Systems; Zeiss).

iPALM

iPALM imaging was performed as previously described (Kanchanawong et al., 2010; Shtengel et al., 2009). Briefly, cells were cultured on 25 mm diameter round coverslips containing gold nanorod fiducial markers (Nanopartz, Inc.), passivated with a ca. 50 nm layer of SiO2, deposited using a Denton Explorer vacuum evaporator. After fixation, an 18 mm coverslip was adhered to the top of the sample and placed in the iPALM. mEos tagged samples were excited using 561 nm laser excitation at ca. 1-2 kW/cm^2 intensity in TIRF conditions. Photoconversion of mEos was performed using 405 nm laser illumination at 2-10 W/cm^2 intensity. 40,000-80,000 images were acquired at 50 ms exposure, and processed/localized using the PeakSelector software (Janelia Research Campus). Alexa Fluor 647 labeled samples were imaged similarly, but with 2-3 kW/cm^2 intensity 647 nm laser excitation, and 30-40 ms exposure time in STORM-buffer containing TRIS-buffered glucose, glucose oxidase, catalase, and mercaptoethanol amine (Dempsey et al., 2011).

iPALM data were analysed and images rendered using the PeakSelector software (Janelia Research Campus) as previously described (Kanchanawong et al., 2010; Shtengel et al., 2009). In short, iPALM images were rendered using a single colour scheme from red to purple, covering the Z range 0-200 nm, where features within focal adhesions are seen. The same colour scheme was also used

for side-view (xz) images. As iPALM localization data records both the fluorescent molecules localized within the focal adhesions as well as molecules in the cytoplasmic fraction, to quantify the spatial distribution of the proteins within individual focal adhesion, we zoomed into areas covered only by the focal adhesion and the immediately surrounding space. To render iPALM images, a single colour scheme was used from red to purple, covering the Z range 0-200 nm, where features within focal adhesions are seen. The same colour scheme was also used for side-view (xz) images. For analysis of protein distributions in focal adhesions: Z_{centre} and S_{vert} calculation, the three-dimensional molecular coordinates for each region (individual focal adhesion) were analysed to obtain histograms of vertical positions with 1-nm bins. The centre vertical positions (Z_{centre}) and width (S_{vert}) were determined from a Gaussian fit to the focal adhesion molecule peak. For proteins like actin and α-actinin were dual peaks were observed, the fitting was done using the sum of two-Gaussian distributions with independent centre vertical position and width. After the histograms for all images and individual focal adhesions were obtained, they were combined into a single average Z_{centre} and S_{vert}.

Quantification of focal adhesion properties

For the quantification of focal adhesion area, the FA number, density and characteristic area were analysed using the ImageJ software (NIH) in a similar way as previously described (Närvä et al., 2017). In short, individual FAs were first identified and measured using the 'analyze particles' built-in function of ImageJ. Second, as we observed that the distribution of FA area was not Gaussian but rather a heavy-tailed distribution, this was approximated and fitted in Igor Pro (WaveMetrics) to a hyper-exponential distribution, or in other words a weighted sum of two exponential densities. Finally, the fit provided us with two characteristic areas of FAs for each curve, A1 describing the smaller FAs and A2 describing the larger FAs. As A1 was not significantly different between samples, we focused on the differences found on A2 that describes the larger FAs rarely present in fibroblasts or at the center of hiPSC colonies, but regularly present at the edge of hiPSC colonies. For simplicity, throughout the paper the characteristic area A2 is referred to as 'characteristic FA area'. In the case of hiPSC colonies, as there were clear visible differences in the FA size at the edge of the colony, we separated the edge from the center for quantification. The edge was defined as a 40-pixel-thick strip starting from the line delimiting the colony boundary and extending towards the inside of the colony. The centre was defined as the remaining region of the colony.

Statistical analysis

If not indicated otherwise, statistical analyses were performed using an analysis of variance (ANOVA) complemented by Tukey's honest significant difference test (Tukey's HSD). The software R version 3.3.3 (R Development Core Team, Vienna, Austria) was used to perform these analyses. Statistical significance levels are annotated as ns = non significant ($p > 0.05$) or providing the range of p value.

Data availability

The authors declare that the data supporting the findings of this study are available within the article and from the authors on request.

Ethical Considerations

The hiPSC lines have been derived under the approval of the Coordinating Ethics Committee of Helsinki and Uusimaa Hospital District (statement nr. 423/13/03/00/08).

Acknowledgements

We thank J. Siivonen and P. Laasola for technical assistance. We thank Michael Davidson, Feng Zhang, Reinhard Fässler, Janet Askari, Martin Humphries and The Allen Institute for Cell Science for providing reagents. The Cell Imaging Core (Turku Centre for Biotechnology, University of Turku, Åbo Akademi University and Biocenter Finland) and the functional genomics unit of the University of Helsinki (Research Programs Unit, HiLIFE Helsinki Institute of Life Science, Faculty of Medicine, University of Helsinki, Biocenter Finland) are acknowledged for services, instrumentation, and expertise.

iPALM imaging was performed in collaboration with the Advanced Imaging Center at Janelia Research Campus, a facility jointly supported by the Gordon and Betty Moore foundation and the Howard Hughes Medical Institute.

Funding:

This study has been supported by the Academy of Finland (G.J., E.N. and J.I.), Academy of Finland CoE for Translational Cancer Research (J.I.), ERC CoG grant 615258, Sigrid Juselius Foundation and the Finnish Cancer Organization (J.I.). A.S. has been supported by the University of Turku

Doctoral programme for Molecular Medicine (TuDMM). iPALM microscopy was performed at the Howard Hughes Medical Institute (HHMI) Janelia Research Campus Advanced Imaging Center (AIC). The AIC is jointly sponsored by the HHMI and the Gordon and Betty Moore Foundation.

Authors contributions

Conceptualization, J.I., C.G. and A.S.; Methodology, A.S., C.G., E.N., J.A., G.J. ; Formal Analysis, C.G., A.S., E.N., J.A.; Investigation, A.S., C.G., E.N., J.A., M.S., J.I.; Resources, M.M.; Writing–Original Draft, C.G., J.I., G.J.; Writing – Review and Editing, C.G., A.S., E.N., J.I., G.J.; Visualization, C.G., A.S., G.J.; Supervision, J.I. and T-L.C.; Funding Acquisition, J.I.

Conflicts of interests

The authors declare no competing financial interests.

References

Askari, J.A., P.A. Buckley, A.P. Mould, and M.J. Humphries. 2009. Linking integrin conformation to function. *J. Cell Sci.* 122:165–170. doi:10.1242/jcs.018556.

Baxter, M.A., M.V. Camarasa, N. Bates, F. Small, P. Murray, D. Edgar, and S.J. Kimber. 2009. Analysis of the distinct functions of growth factors and tissue culture substrates necessary for the long-term self-renewal of human embryonic stem cell lines. *Stem Cell Res.* 3:28–38. doi:10.1016/j.scr.2009.03.002.

Bouchet, B.P., R.E. Gough, Y.-C. Ammon, D. van de Willige, H. Post, G. Jacquemet, A.M. Altelaar, A.J. Heck, B.T. Goult, and A. Akhmanova. 2016. Talin-KANK1 interaction controls the recruitment of cortical microtubule stabilizing complexes to focal adhesions. *eLife*. 5:e18124. doi:10.7554/eLife.18124.

Bouissou, A., A. Proag, N. Bourg, K. Pingris, C. Cabriel, S. Balor, T. Mangeat, C. Thibault, C. Vieu, G. Dupuis, E. Fort, S. Lévêque-Fort, I. Maridonneau-Parini, and R. Poincloux. 2017. Podosome Force Generation Machinery: A Local Balance between Protrusion at the Core and Traction at the Ring. *ACS Nano*. 11:4028–4040. doi:10.1021/acsnano.7b00622.

Boyer, L.A., T.I. Lee, M.F. Cole, S.E. Johnstone, S.S. Levine, J.P. Zucker, M.G. Guenther, R.M. Kumar, H.L. Murray, R.G. Jenner, D.K. Gifford, D.A. Melton, R. Jaenisch, and R.A. Young. 2005. Core Transcriptional Regulatory Circuitry in Human Embryonic Stem Cells. *Cell*. 122:947–956. doi:10.1016/j.cell.2005.08.020.

Braam, S.R., L. Zeinstra, S. Litjens, D. Ward-van Oostwaard, S. van den Brink, L. van Laake, F. Lebrin, P. Kats, R. Hochstenbach, R. Passier, A. Sonnenberg, and C.L. Mummery. 2008. Recombinant vitronectin is a functionally defined substrate that supports human embryonic stem cell self-renewal via alphavbeta5 integrin. *Stem Cells Dayt. Ohio*. 26:2257–2265. doi:10.1634/stemcells.2008-0291.

Carisey, A., and C. Ballestrem. 2011. Vinculin, an adapter protein in control of cell adhesion signalling. *Eur. J. Cell Biol.* 90:157–163. doi:10.1016/j.ejcb.2010.06.007.

Carisey, A., R. Tsang, A.M. Greiner, N. Nijenhuis, N. Heath, A. Nazgiewicz, R. Kemkemer, B. Derby, J. Spatz, and C. Ballestrem. 2013. Vinculin regulates the recruitment and release of core focal adhesion proteins in a force-dependent manner. *Curr. Biol. CB*. 23:271–281. doi:10.1016/j.cub.2013.01.009.

Case, L.B., M.A. Baird, G. Shtengel, S.L. Campbell, H.F. Hess, M.W. Davidson, and C.M. Waterman. 2015. Molecular mechanism of vinculin activation and nano-scale spatial organization in focal adhesions. *Nat. Cell Biol.* 17:880–892. doi:10.1038/ncb3180.

Dempsey, G.T., J.C. Vaughan, K.H. Chen, M. Bates, and X. Zhuang. 2011. Evaluation of fluorophores for optimal performance in localization-based super-resolution imaging. *Nat. Methods*. 8:1027–1036. doi:10.1038/nmeth.1768.

Horton, E.R., A. Byron, J.A. Askari, D.H.J. Ng, A. Millon-Frémillon, J. Robertson, E.J. Koper, N.R. Paul, S. Warwood, D. Knight, J.D. Humphries, and M.J. Humphries. 2015. Definition of a

consensus integrin adhesome and its dynamics during adhesion complex assembly and disassembly. *Nat. Cell Biol.* 17:1577–1587. doi:10.1038/ncb3257.

Humphries, J.D., A. Byron, and M.J. Humphries. 2006. Integrin ligands at a glance. *J. Cell Sci.* 119:3901–3903. doi:10.1242/jcs.03098.

Kanchanawong, P., G. Shtengel, A.M. Pasapera, E.B. Ramko, M.W. Davidson, H.F. Hess, and C.M. Waterman. 2010. Nanoscale architecture of integrin-based cell adhesions. *Nature*. 468:580–584. doi:10.1038/nature09621.

Legate, K.R., S.A. Wickström, and R. Fässler. 2009. Genetic and cell biological analysis of integrin outside-in signaling. *Genes Dev.* 23:397–418. doi:10.1101/gad.1758709.

Liu, J., Y. Wang, W.I. Goh, H. Goh, M.A. Baird, S. Ruehland, S. Teo, N. Bate, D.R. Critchley, M.W. Davidson, and P. Kanchanawong. 2015. Talin determines the nanoscale architecture of focal adhesions. *Proc. Natl. Acad. Sci.* 112:E4864–E4873. doi:10.1073/pnas.1512025112.

Meng, Y., S. Eshghi, Y.J. Li, R. Schmidt, D.V. Schaffer, and K.E. Healy. 2010. Characterization of integrin engagement during defined human embryonic stem cell culture. *FASEB J. Off. Publ. Fed. Am. Soc. Exp. Biol.* 24:1056–1065. doi:10.1096/fj.08-126821.

Mikkola, M., S. Toivonen, K. Tamminen, K. Alfthan, T. Tuuri, T. Satomaa, J. Natunen, J. Saarinen, M. Tiittanen, M. Lampinen, L. Valmu, J. Partanen, and T. Otonkoski. 2013. Lectin from Erythrina cristagalli supports undifferentiated growth and differentiation of human pluripotent stem cells. *Stem Cells Dev.* 22:707–716. doi:10.1089/scd.2012.0365.

Närvä, E., A. Stubb, C. Guzmán, M. Blomqvist, D. Balboa, M. Lerche, M. Saari, T. Otonkoski, and J. Ivaska. 2017. A Strong Contractile Actin Fence and Large Adhesions Direct Human Pluripotent Colony Morphology and Adhesion. *Stem Cell Rep.* 9:67–76. doi:10.1016/j.stemcr.2017.05.021.

Rafiq, N.M., Y. Nishimura, S.V. Plotnikov, V. Thiagarajan, Z. Zhang, M. Natarajan, S. Shi, V. Viasnoff, G.E. Jones, P. Kanchanawong, and A.D. Bershadsky. 2018. The cytoskeleton as a smart composite material: A unified pathway linking microtubules, myosin-II filaments and integrin adhesions. *bioRxiv*. 195495. doi:10.1101/195495.

Ran, F.A., P.D. Hsu, J. Wright, V. Agarwala, D.A. Scott, and F. Zhang. 2013. Genome engineering using the CRISPR-Cas9 system. *Nat. Protoc.* 8:2281–2308. doi:10.1038/nprot.2013.143.

Roberts, B., A. Haupt, A. Tucker, T. Grancharova, J. Arakaki, M.A. Fuqua, A. Nelson, C. Hookway, S.A. Ludmann, I.A. Mueller, R. Yang, R. Horwitz, S.M. Rafelski, and R.N. Gunawardane. 2017. Systematic gene tagging using CRISPR/Cas9 in human stem cells to illuminate cell organization. *Mol. Biol. Cell*. 28:2854–2874. doi:10.1091/mbc.E17-03-0209.

Rodin, S., L. Antonsson, C. Niaudet, O.E. Simonson, E. Salmela, E.M. Hansson, A. Domogatskaya, Z. Xiao, P. Damdimopoulou, M. Sheikhi, J. Inzunza, A.-S. Nilsson, D. Baker, R. Kuiper, Y. Sun, E. Blennow, M. Nordenskjöld, K.-H. Grinnemo, J. Kere, C. Betsholtz, O. Hovatta, and K. Tryggvason. 2014. Clonal culturing of human embryonic stem cells on laminin-521/E-cadherin matrix in defined and xeno-free environment. *Nat. Commun.* 5:3195. doi:10.1038/ncomms4195.

Rossier, O., V. Octeau, J.-B. Sibarita, C. Leduc, B. Tessier, D. Nair, V. Gatterdam, O. Destaing, C. Albigès-Rizo, R. Tampé, L. Cognet, D. Choquet, B. Lounis, and G. Giannone. 2012. Integrins β1 and β3 exhibit distinct dynamic nanoscale organizations inside focal adhesions. *Nat. Cell Biol.* 14:1057–1067. doi:10.1038/ncb2588.

Shtengel, G., J.A. Galbraith, C.G. Galbraith, J. Lippincott-Schwartz, J.M. Gillette, S. Manley, R. Sougrat, C.M. Waterman, P. Kanchanawong, M.W. Davidson, R.D. Fetter, and H.F. Hess. 2009. Interferometric fluorescent super-resolution microscopy resolves 3D cellular ultrastructure. *Proc. Natl. Acad. Sci.* 106:3125–3130. doi:10.1073/pnas.0813131106.

Spiess, M., P. Hernandez-Varas, A. Oddone, H. Olofsson, H. Blom, D. Waithe, J.G. Lock, M. Lakadamyali, and S. Strömblad. 2018. Active and inactive β1 integrins segregate into distinct nanoclusters in focal adhesions. *J. Cell Biol.* 217:1929–1940. doi:10.1083/jcb.201707075.

Sun, Z., H.-Y. Tseng, S. Tan, F. Senger, L. Kurzawa, D. Dedden, N. Mizuno, A.A. Wasik, M. Thery, A.R. Dunn, and R. Fässler. 2016. Kank2 activates talin, reduces force transduction across integrins and induces central adhesion formation. *Nat. Cell Biol.* 18:941–953. doi:10.1038/ncb3402.

Takahashi, K., K. Tanabe, M. Ohnuki, M. Narita, T. Ichisaka, K. Tomoda, and S. Yamanaka. 2007. Induction of pluripotent stem cells from adult human fibroblasts by defined factors. *Cell*. 131:861–872. doi:10.1016/j.cell.2007.11.019.

Thomson, J.A., J. Itskovitz-Eldor, S.S. Shapiro, M.A. Waknitz, J.J. Swiergiel, V.S. Marshall, and J.M. Jones. 1998. Embryonic stem cell lines derived from human blastocysts. *Science*. 282:1145–1147.

Trokovic, R., J. Weltner, and T. Otonkoski. 2015. Generation of iPSC line HEL24.3 from human neonatal foreskin fibroblasts. *Stem Cell Res.* 15:266–268. doi:10.1016/j.scr.2015.05.012.

Yao, M., B.T. Goult, H. Chen, P. Cong, M.P. Sheetz, and J. Yan. 2014. Mechanical activation of vinculin binding to talin locks talin in an unfolded conformation. *Sci. Rep.* 4:4610. doi:10.1038/srep04610.

Yao, M., B.T. Goult, B. Klapholz, X. Hu, C.P. Toseland, Y. Guo, P. Cong, M.P. Sheetz, and J. Yan. 2016. The mechanical response of talin. *Nat. Commun.* 7:11966. doi:10.1038/ncomms11966.

Yu, J., M.A. Vodyanik, K. Smuga-Otto, J. Antosiewicz-Bourget, J.L. Frane, S. Tian, J. Nie, G.A. Jonsdottir, V. Ruotti, R. Stewart, I.I. Slukvin, and J.A. Thomson. 2007. Induced pluripotent stem cell lines derived from human somatic cells. *Science*. 318:1917–1920. doi:10.1126/science.1151526.

Figure Legends

Figure 1: Constraint of cornerstone adhesion compromise pluripotency

(a-b) hPSC cells plated for 24 h on a VTN-coated uniform surface (**a**) or on a VTN-coated nano-grated nanopattern in E8 medium (**b**), were stained for F-actin, paxillin and dapi. Images were acquired using an AiryScan confocal microscope. Scale bars 10 µm. ROI denote regions of interests. (**c**): Cartoon highlighting the topography of the nano-grated nanopattern used. **(d-e)** Representative western blot (**d**) and quantification (**e**) of Sox2 levels in human embryonic fibroblast (hEF) and in hPSC plated for three days either on VTN-coated uniform surfaces in presence or absence of BMP4 or on VTN-coated nano-grated nanopatterns (n= 3). **(f)** hPSC cells plated for three days either on VTN-coated uniform surfaces (using E6 medium) in presence or absence of BMP4 or on VTN-coated nano-grated nanopatterns, were stained for SSEA-1 and dapi. Images were acquired using an SDC confocal microscope using a 20x objective (n= 3). Scale bars 50 µm.

Figure 2: Lateral and vertical segregation of proteins within cornerstone FA.

(**a-c**) Interferometric photo-activated localization microscopy (iPALM) images of integrin β5 (**a**), paxillin (**b**) and talin-1 (N-terminally tagged talin-1, **c**) in cornerstone FA. Both top-view (XY) and side-view (XZ) images of the indicated proteins are displayed. White boxes indicate the area used to generate the side-view images. For all images, individual localisations are colour-coded as a function of their Z-positioning (distance from the coverslip). (**d**) hPSC cells plated for 24 h on VTN were stained for integrin β5 and active integrin β1 (mAb 12G10) and imaged using an AiryScan confocal microscope. The yellow line highlights the area used to measure the intensity profiles displayed on the side.

(**e**): Schematic representation of the different layers previously identified in FA using IPALM (Kanchanawong et al., 2010). The integrin signalling layer is highlighted. (**f**): Z positioning (distance from the coverslip, Z_{centre}) of integrin αV, integrin β5 and paxillin in cornerstone adhesions as measured using IPALM. Boxes display the median, plus the 1st and 3rd quartiles (IQR: 25th– 75th percentile). Whiskers correspond to the median ± 1.5 x IQR.

Figure 3: Vinculin distribution and orientation within cornerstone adhesions

(**a**) Schematic representation of the different layers previously identified in FA using IPALM. The force transduction layer containing vinculin and talin is highlighted. (**b**) Z positioning (distance from the coverslip, Z_{centre}) of N-terminally (Talin-1-N) and C-terminally (Talin-1-C) tagged talin-1 in cornerstone adhesions. Results are displayed as boxplots as in figure 2f. (**c**) Z positioning (distance from the coverslip, Z_{centre}) of N-terminally (Vinculin-N) and C-terminally (Vinculin-C) tagged vinculin in cornerstone adhesions. Results are displayed as boxplots as in figure 2f. (**d**) Two-colour iPALM images of vinculin (Vinculin-C) and endogenous paxillin in a cornerstone FA. As in figure 2A, both top-view (top panels) and side-view (bottom panels) images are displayed. Localisation of vinculin and paxillin are displayed separately (images colour-coded as a function of their Z-positioning) and together (overlay, colours represent individual molecules). Scale bar 1 µm. **(e)** 3D scatter plots displaying the individual iPALM localizations (grey dots) of paxillin, N-terminally (Vinculin-N) and C-terminally (Vinculin-C) tagged vinculin within a single cornerstone adhesion. Surface plots present the fit of those localisations using a two-dimensional polynomial equation. Note that the paxillin localisations are homogeneously flats while localisations of both vinculin constructs form a solid paraboloid. **(f)** iPALM XY images of selected Z-layers of an individual FA labelled for vinculin-C. Scale bar 1 µm.

Figure 4: Actin and α-actinin-1 lateral distribution

(a) Schematic representation of the different layers previously identified in FA using IPALM. The actin regulatory layer containing actin and α-actinin-1 is highlighted. **(b)** Two-color iPALM images of actin and endogenous paxillin in cornerstone FA. As in figure 2A, both top-view (top panels) and side-view (bottom panels) images are displayed. The localisations of actin are displayed separately (image colour-coded as a function of the Z-positioning) and together with paxillin (overlay, colours represent individual molecules). Scale bar 1 µm. **(c)** Z-density profile of paxillin (red) and actin (green) displaying the number of localisations as a function of the Z-position in an individual cornerstone adhesion. Dotted lines correspond to the experimental data while continuous lines correspond to the fitted data obtained using either a single Gaussian distribution (paxillin) or a sum of two Gaussian distributions (actin). Dashed black lines highlight these two Gaussian distributions. **(d)** iPALM image of α-actinin-1 in an individual cornerstone FA. As in figure 2A, individual localisations are colour-coded as a function of their Z-positioning and both top-view (top panel) and side-view (bottom panel) images are displayed. Scale bar 1 µm. **(e)** Z-density profile of α-actinin-1 (purple) showing the number of localisations as a function of the Z-position. Dotted line

corresponds to the experimental data while the continuous line corresponds to the fitted data obtained using a sum of two Gaussian distributions (Dashed black lines). **(f)** Z positioning (distance from the coverslip, Z_{centre}) of actin and α-actinin-1 in cornerstone adhesions. “low” and “high” denote separate peaks in the distribution of the same protein. Results are displayed as boxplots where boxes display the median, plus the 1st and 3rd quartiles (IQR: 25th– 75th percentile). Whiskers correspond to the median ± 1.5 x IQR.

Figure 5: 3D localization of kank1 and kank2 in hPSC at the nanoscale

(a-c) Two-colour iPALM images of endogenous paxillin together with kank1 (**a-b**) or kank2 (**c-d**) in the vicinity of cornerstone FA. For each panels both top-view and side-view images are displayed. In addition, localisation of kank1 or kank2 are displayed separately (images colour-coded as a function of their Z-positioning) and together with paxillin (overlay, colours represent individual molecules). Scale bars 1 µm. (**a**) Example image where kank1 form a wall surrounding a cornerstone FA. (**b-c**) Example images where kank1 (**b**) and kank2 (**c**) localise both in proximity and distally from cornerstone adhesions. Side view images of the highlighted regions of interests are displayed. **(d)** Z positioning (Z_{centre}) of kank1 and kank2 when in proximity to cornerstone adhesion (adjacent to FA) or when distant to cornerstone FA. (**e**) kank1 and kank2 proteins levels in hPSC previously treated with either CTRL siRNA (siCTRL) or a combination of siRNA targetting kank1 and kank2 (siK1 + siK2). (**f**) Quantification of the characteristic FA area at the edges (edge) or in the middle (centre) of hPSC colonies previously treated with CTRL siRNA (siCTRL) or a combination of siRNA targetting kank1 and kank2 (siK1 + siK2) (n= 3).

Figure 6: Overall vertical stratification of cornerstone FA

(**a**) Z positioning (Z_{centre}) of αV and β5 integrins, paxillin, vinculin, talin-1, actin, α-actinin-1, kank1 and kank2 in cornerstone adhesions. Letters –N and –C denote the location of the tag while “low” and “high” denote separate peaks in the distribution of the same protein. Results are displayed as boxplots where boxes display the median, plus the 1st and 3rd quartiles (IQR: 25th– 75th percentile). Whiskers correspond to the median ± 1.5 x IQR. (**d**) Schematic model of the 3D architecture of hPSC cornerstone adhesions. Proteins lateral and vertical positioning is based on the data presented here. This model does not depict protein stoichiometry.

Supplemental material

Supplementary Figure 1: hPSC cornerstone adhesions

(a) Spinning disk (SD) images of hPSC plated on VTN and stained for F-actin, paxillin, dapi and the pluripotency marker nanog. Scale bar 10 µm. **(b)** Live cell imaging of endogenously-tagged paxillin hPSC. Images were acquired using a SD microscope. The full video is available as supplementary information (Video 1). White square highlight regions of interests which are magnified (ROI size 30µm). Several time points of interest as well as temporal code images are displayed. White colour indicate stable adhesions. **(c)** Structure illumination microscopy (SIM) images of hPSC plated on VTN and stained for filamentous actin (F-actin) and paxillin. Scale bar 10 µm. White square highlights a region of interests which is magnified.

Supplementary Figure 2: Adhesion protein levels in hPSC cells

(a) Western blot analysis of endogenous focal adhesion components in U2OS cells and hPSCs grown on VTN for 24h. Oct4 was used as a pluripotency marker and β-actin as a loading control. **(b)** Adhesion proteins level in hPSC compared to U2OS. Quantifications were first normalised to the loading control β-actin then to the level measured in U2OS cells (n=3).

Supplementary Figure 3: Endogenous straining of multiple adhesion proteins in hPSC

Spinning disk (SD) images of hPSC plated on VTN and stained for paxillin, vinculin, β5 integrin, talin, kank1, α-actinin-1, nanog and dapi. White squares highlight regions of interests which are magnified. Scale bar 10 µm.

Supplementary Figure 4: Validation of the constructs used for iPALM

Spinning disk images of hPSC plated on VTN and transiently expressing various Eos-constructs used for iPALM in this study. Red dotted line highlight the nucleus. Oct4 and paxillin were used as a pluripotency and FA markers respectively. Scale bar 10µm.

Supplementary Figure 5: lateral segregation of proteins within cornerstone adhesions

(a-b) Spinning disk image of hPSC plated on VTN and stained for talin and paxillin. Scale bar 10µm. The yellow line highlights the area used to measure the intensity profiles displayed in **(b)**.

(**c-d**) Total internal reflection fluorescence microscopy images of hPSC plated on VTN and stained for αV β5 integrin and paxillin. Scale bar 10 µm. The yellow line highlights the area used to measure the intensity profiles displayed in **(d)**.

Supplementary Figure 6: Vinculin and cornerstone FA

(**a**) iPALM images of vinculin (vinculin-N) in cornerstone FA. As in figure 2A, individual localisations are colour-coded as a function of their Z-positioning and both top-view and side-view images are displayed. Scale bar 1 µm. **(b)** Vinculin, Oct4 and gapdh protein levels in hPSC previously infected with lentivirus containing CTRL shRNA (shCTRL) or two individual shRNA targetting vinculin (shVin#1 and shVin#2). **(c)** Spinning disk images of shCTRL or shVinculin hPSC plated on VTN and stained for paxillin, F-actin and dapi. Scale bar 10 µm. **(d)** Quantification of the characteristic focal adhesion area and the focal adhesion density at the edge and at the centre of shCTRL and shVinculin hPSC colonies (n= 3, see methods for details).

Supplementary Figure 7: kank1 and kank2 in cornerstone FA

(a) Spinning disk images of siCTRL or sikank1 and sikank2 (siK1 + siK2) hPSC plated on VTN and stained for paxillin, F-actin and dapi. Scale bar 10 µm. **(b)** Quantification of the focal adhesion density at the edge and at the centre of s siCTRL or sikank1 and sikank2 hPSC colonies (n= 3, see methods for details).

Movie 1: paxillin dynamics in a hPSC colony plated on vitronectin

Live cell imaging of endogenously-tagged paxillin hPSC. Images were acquired using a SD microscope.

Movie 2: kank1 localisation at the nanoscale in cornerstone adhesion

3D reconstruction of kank1 (green) and paxillin (red) iPALM data highlighting that kank1 assemble a wall surrounding paxillin positive adhesions.

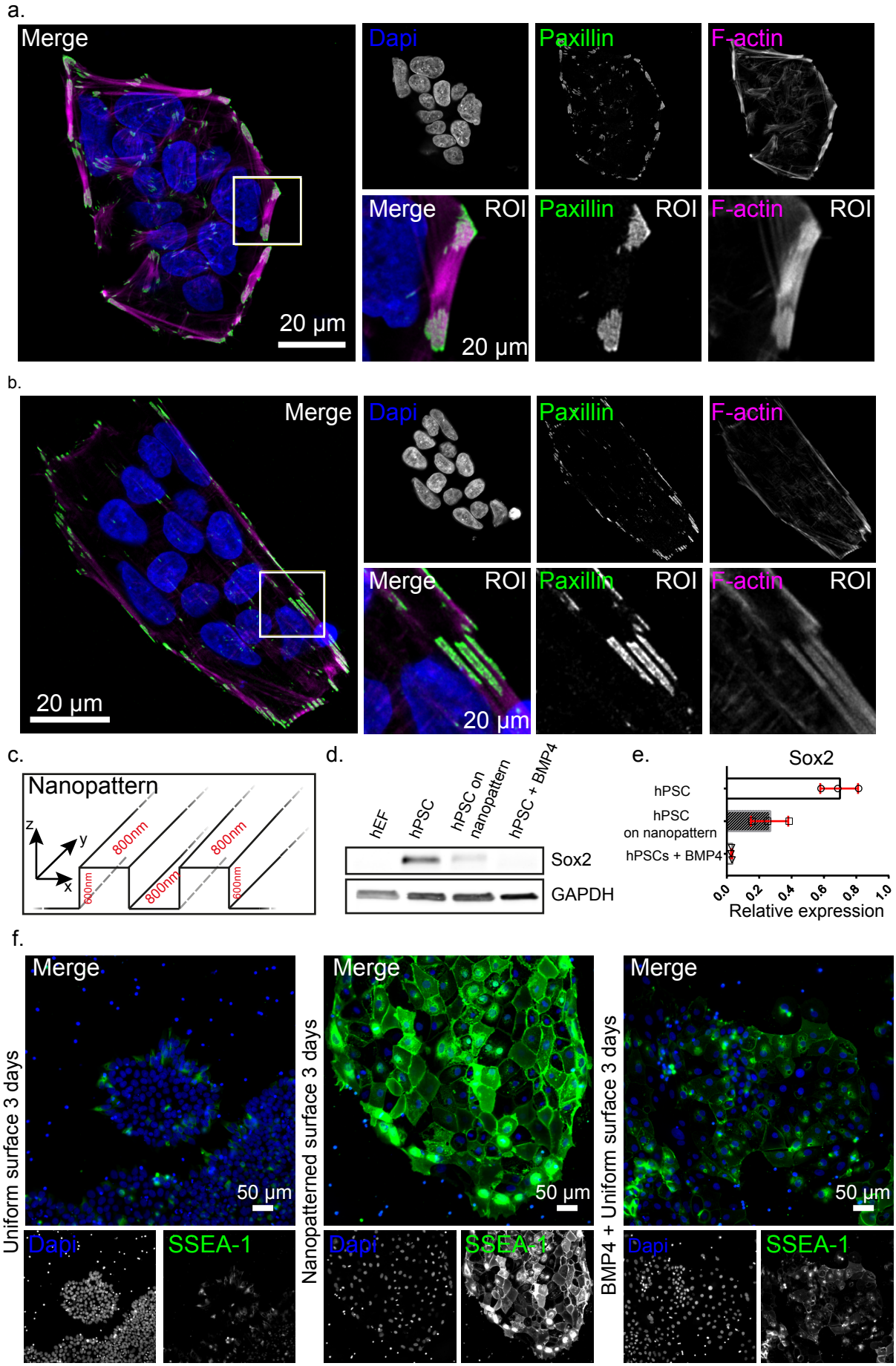

Stubb, Guzmán et al. Figure 1

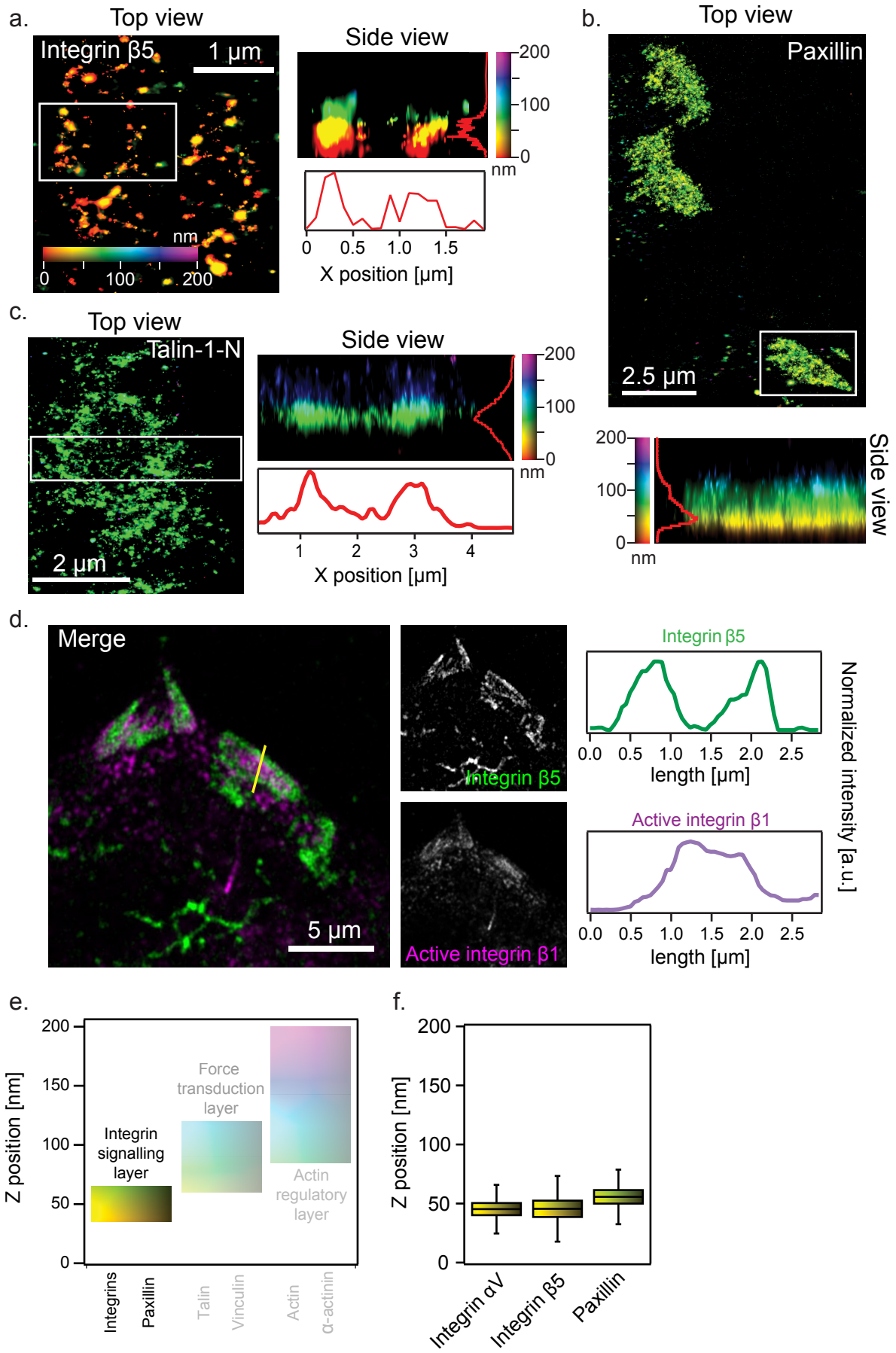

Stubb, Guzmán et al. Figure 2

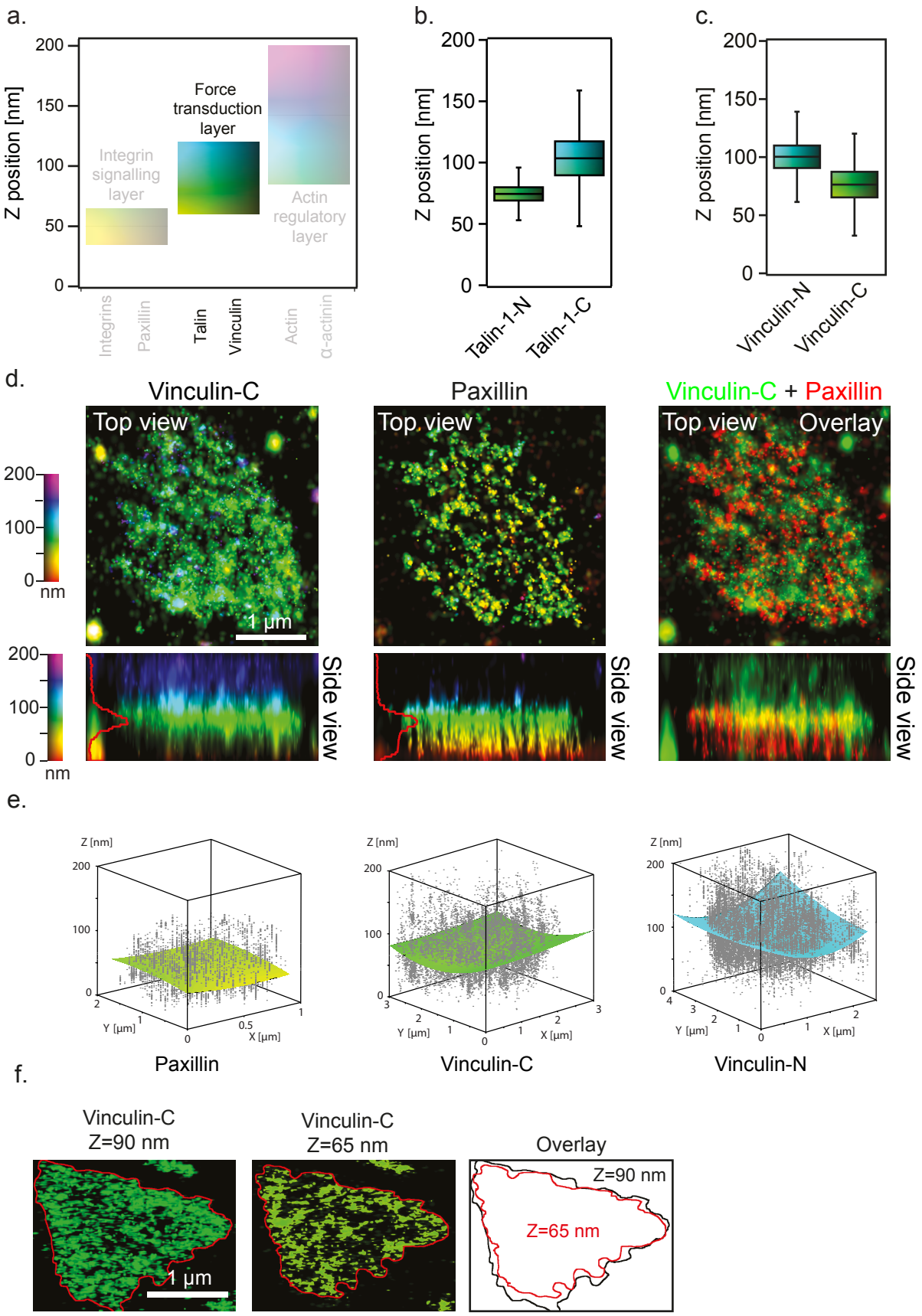

Stubb, Guzmán et al. Figure 3

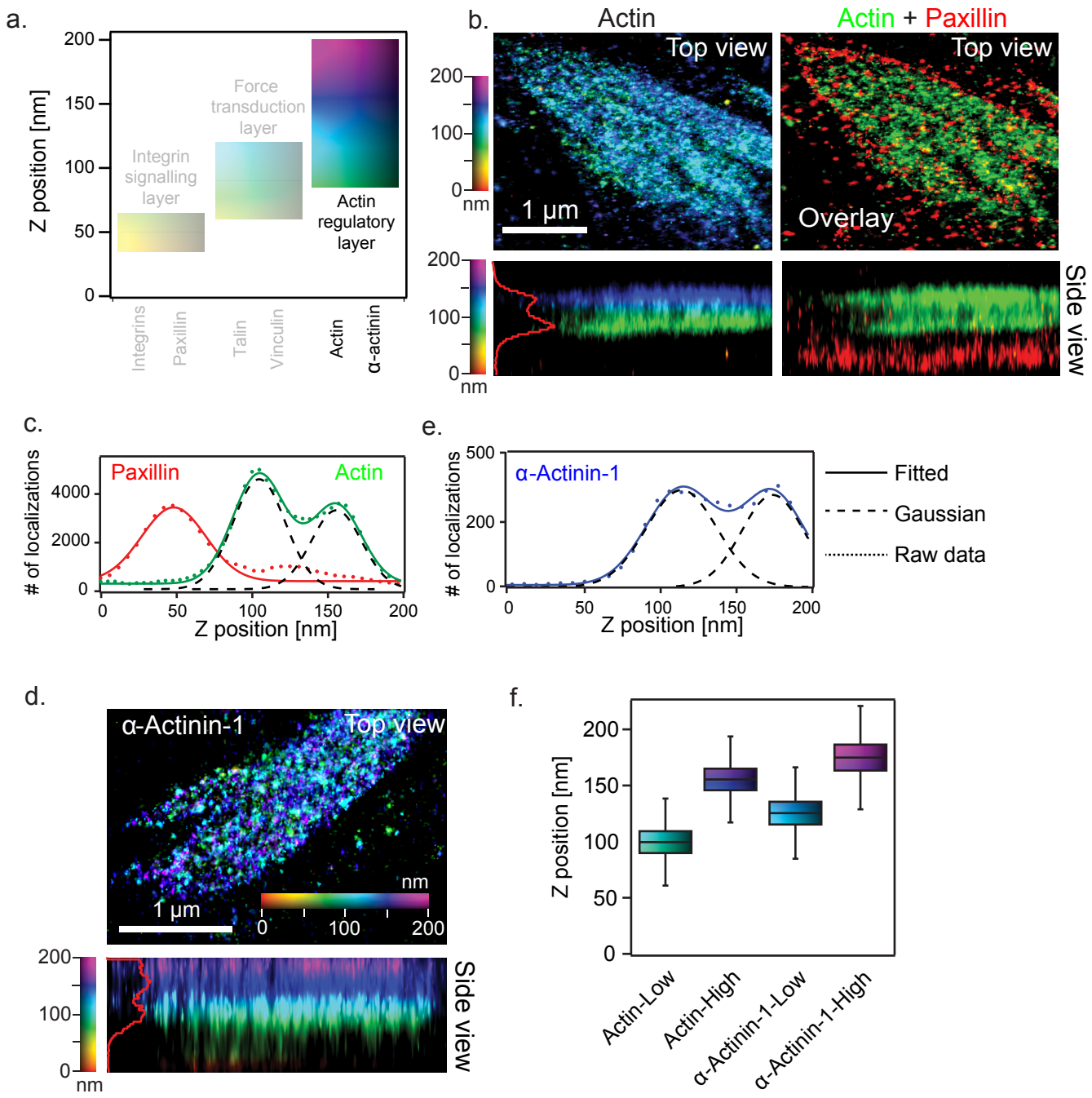

Stubb, Guzmán et al. Figure 4

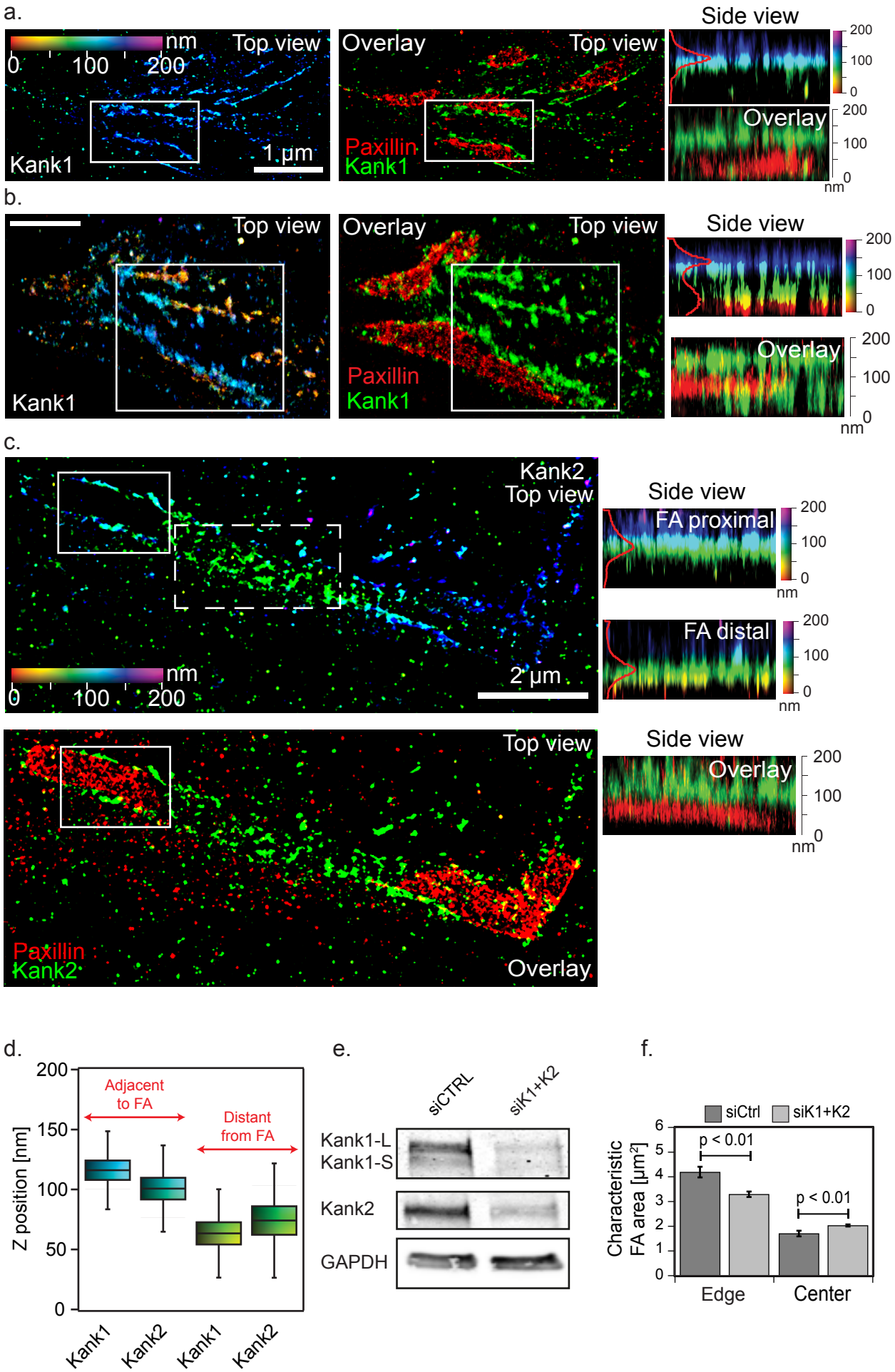

Stubb, Guzmán et al. Figure 5

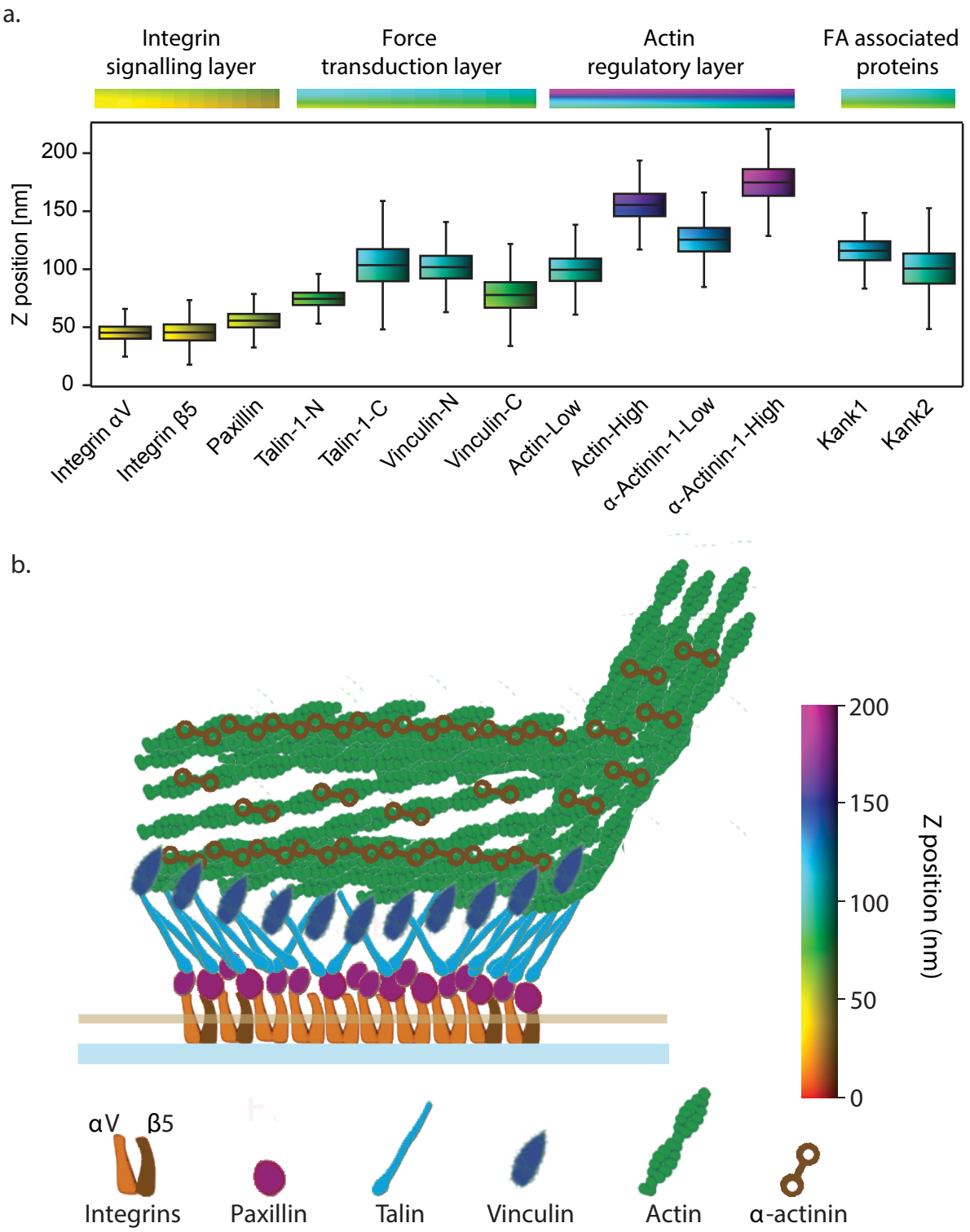

Stubb, Guzman et al. Figure 6

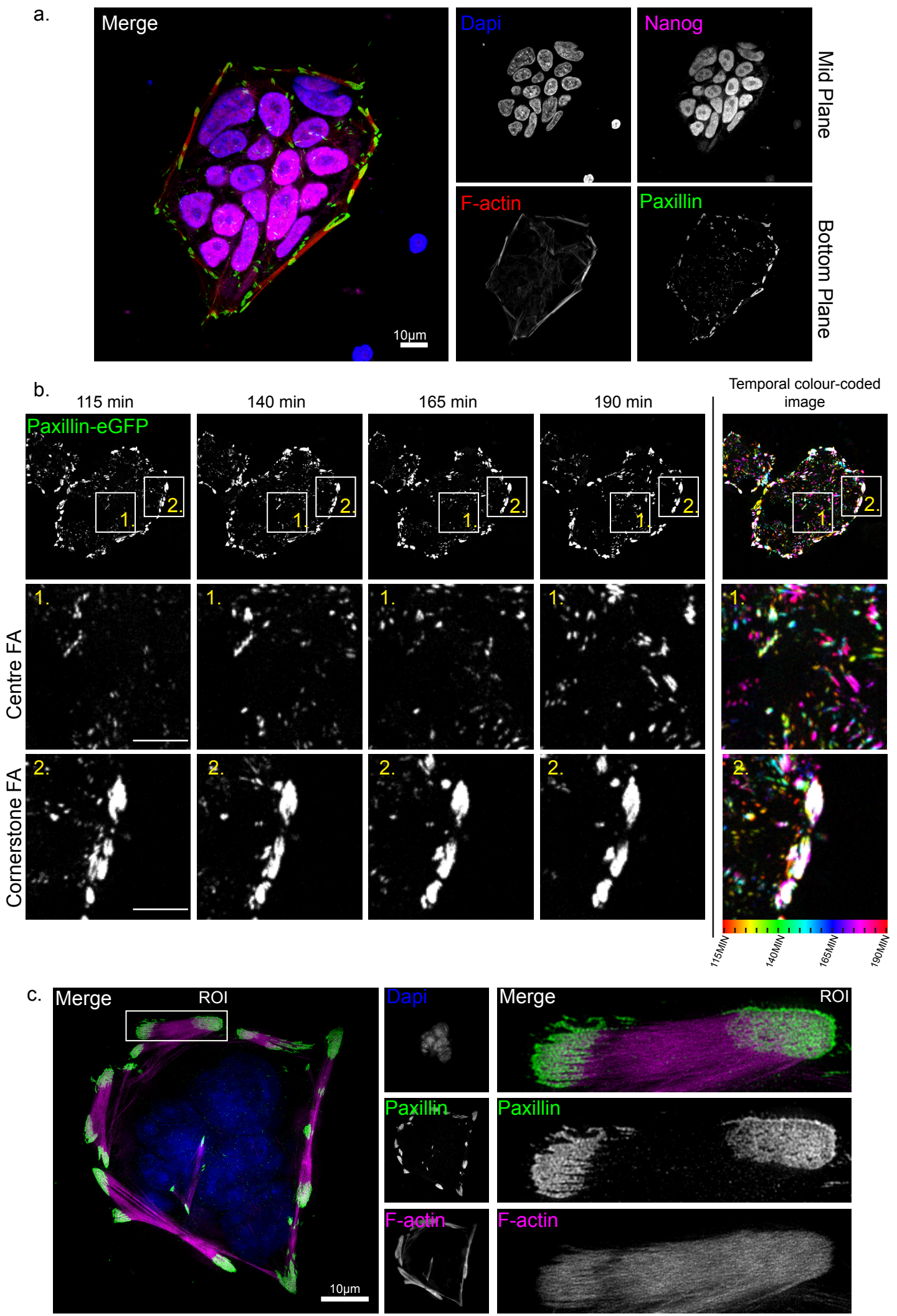

Stubb, Guzmán et al. Supplementary Figure 1

a.

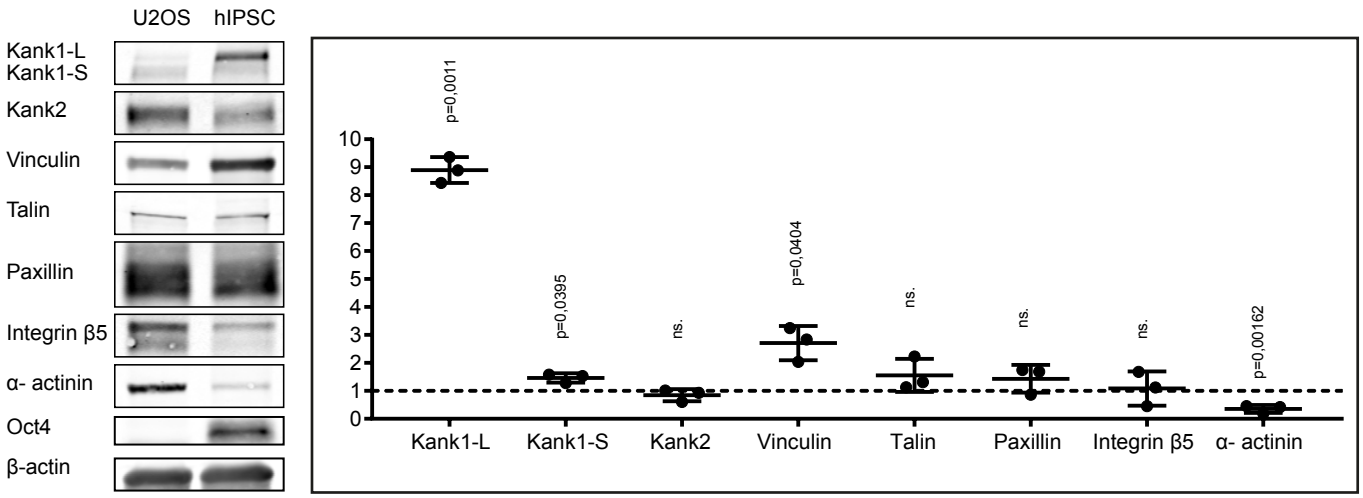

Stubb, Guzmán et al. Supplementary Figure 2

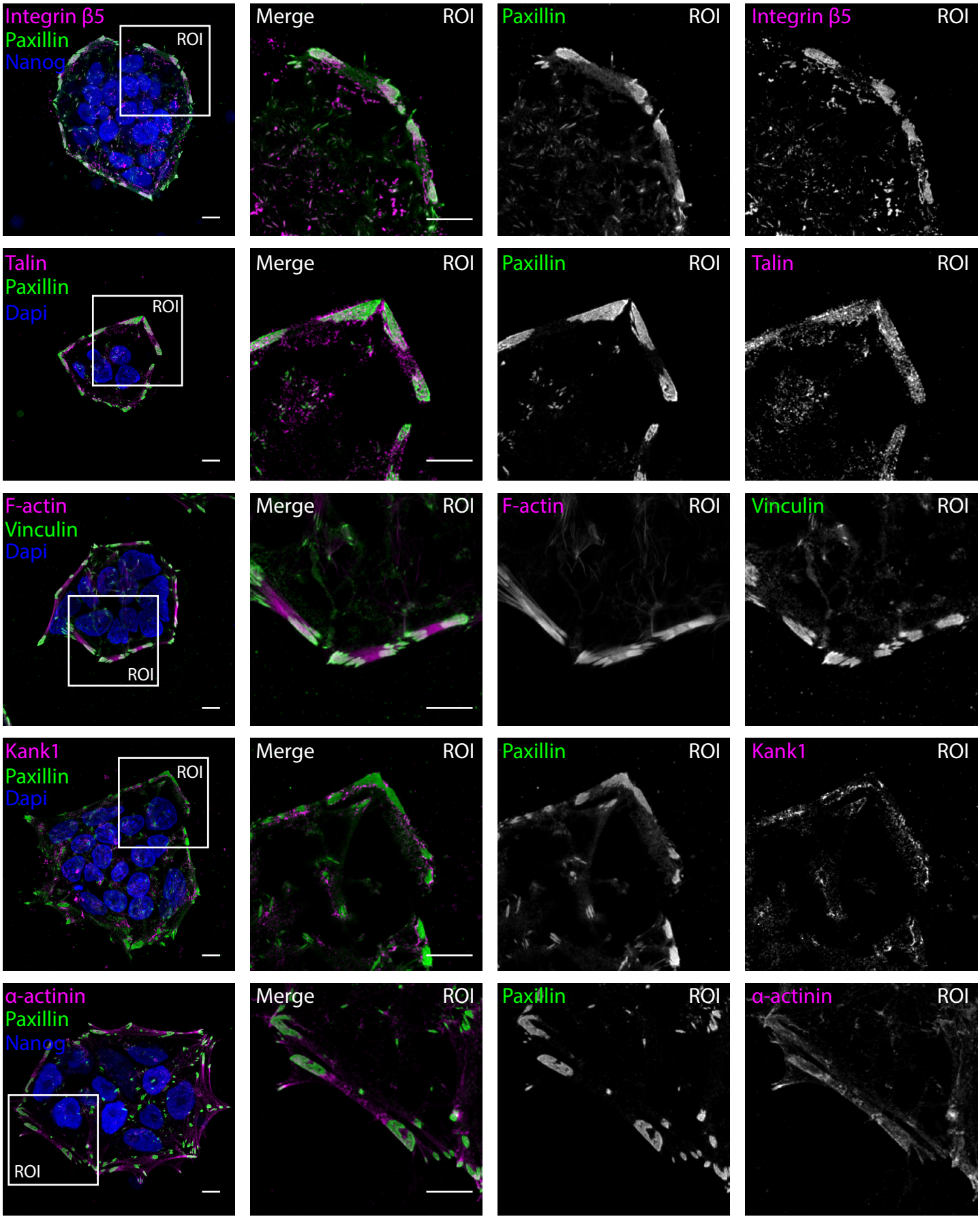

Stubb, Guzmán et al. Supplementary Figure 3

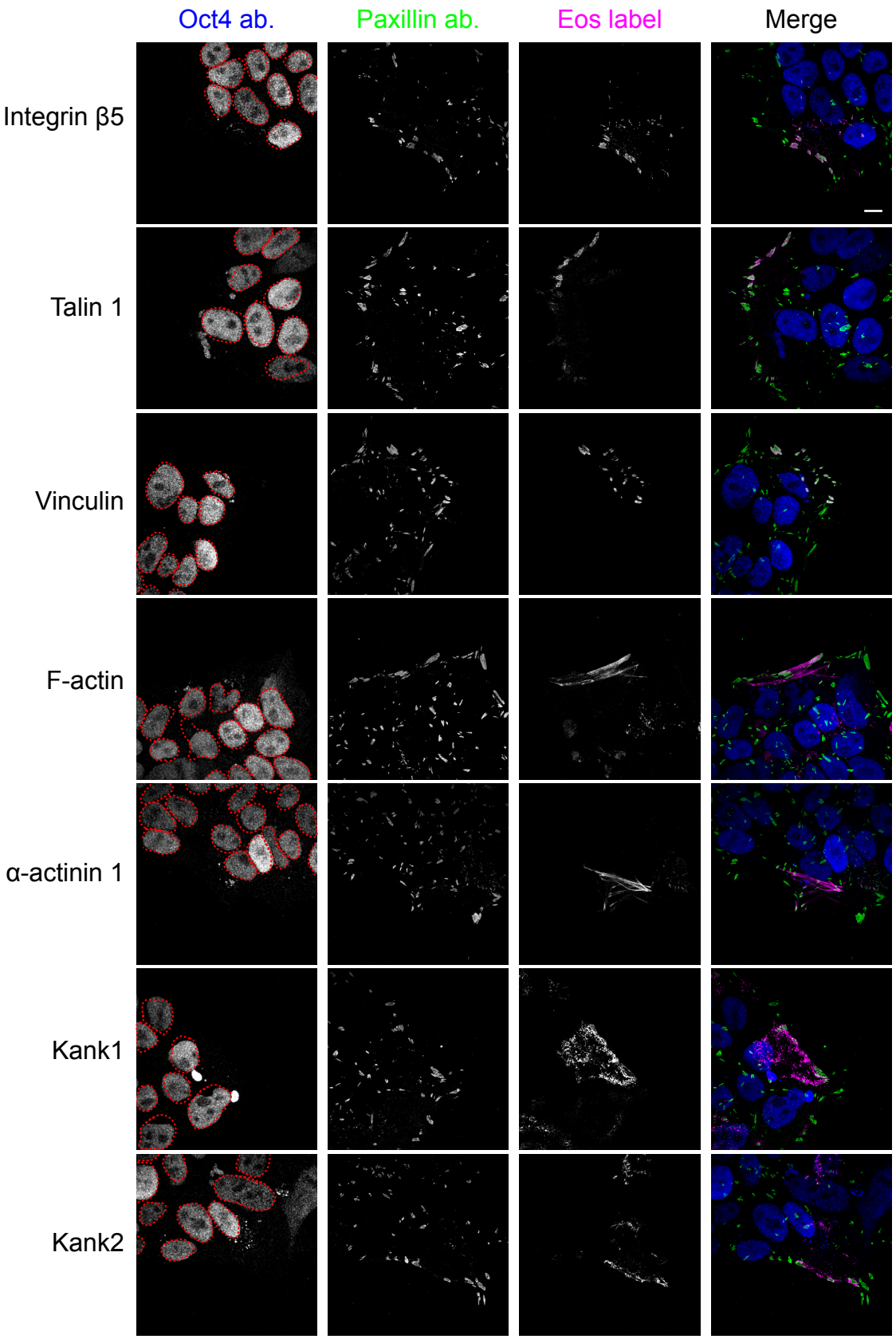

Stubb, Guzmán et al. Supplementary Figure 4

a.

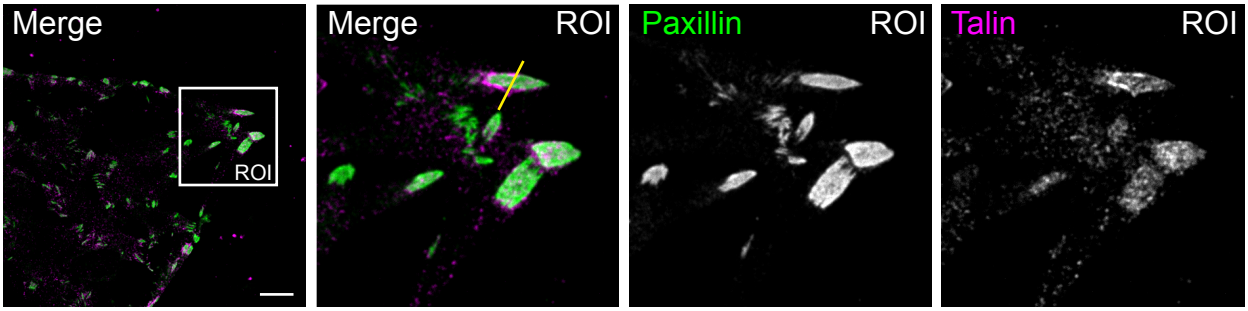

b.

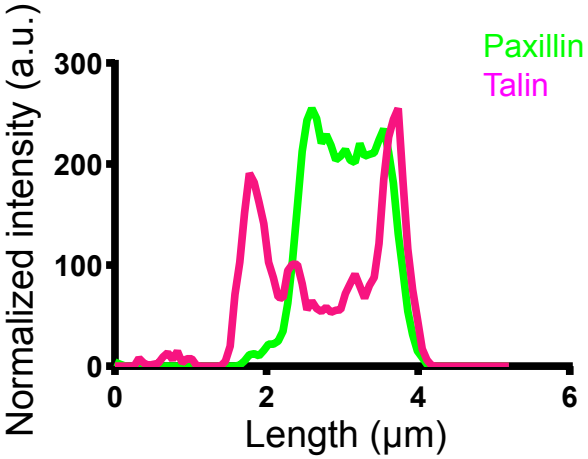

c.

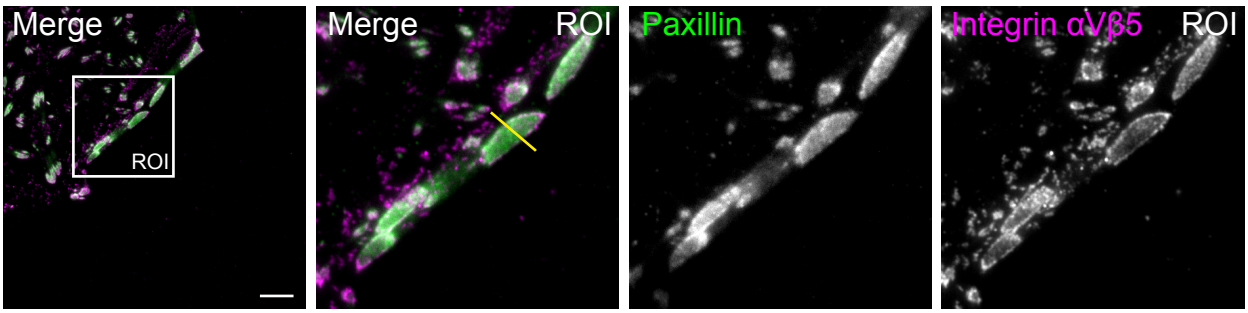

d.

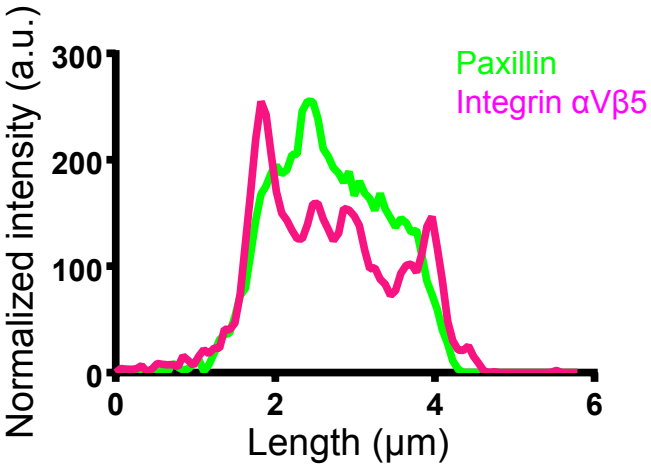

Stubb, Guzmán et al. Supplementary Figure 5

a.

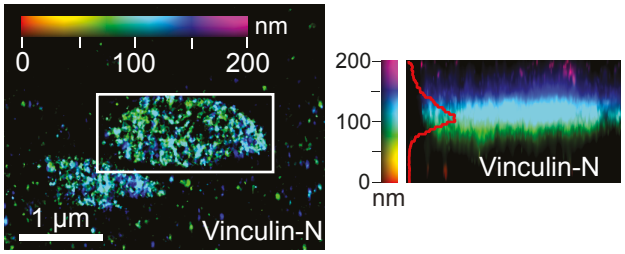

b.

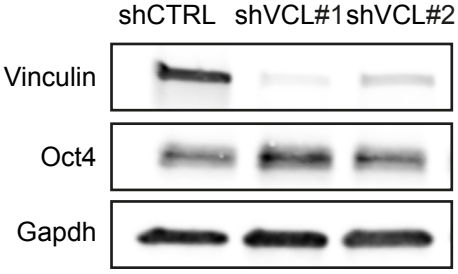

c.

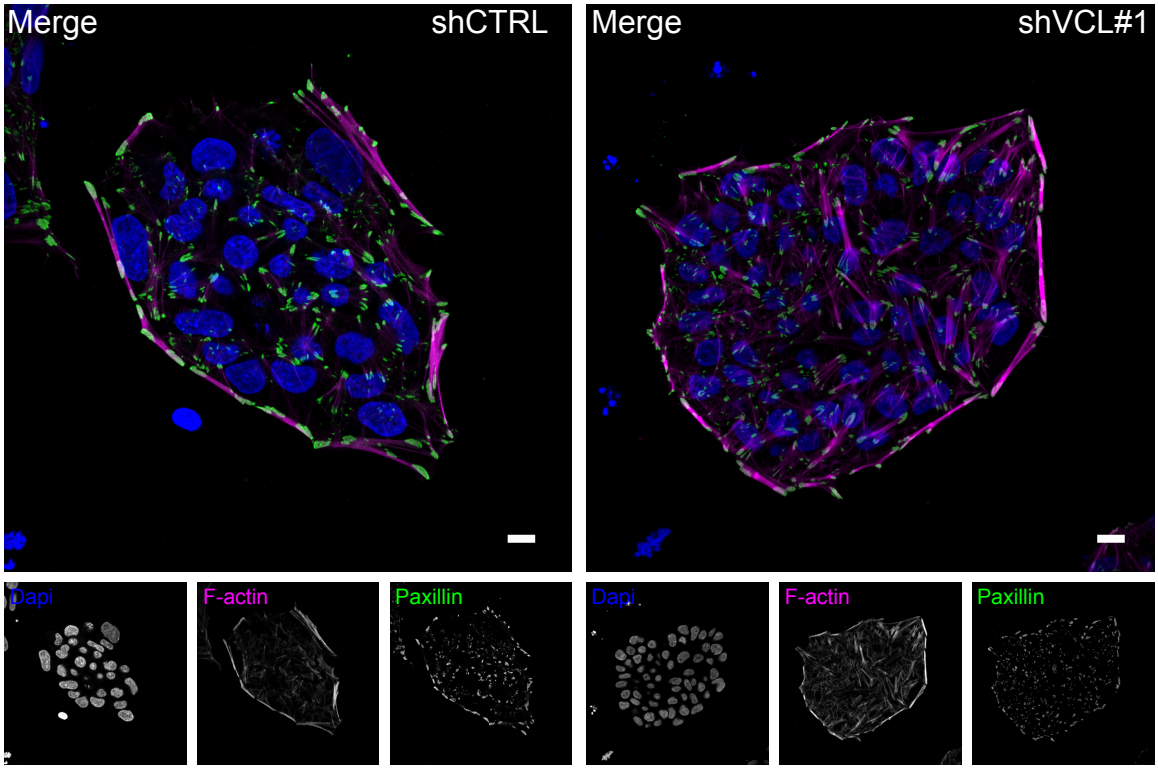

d.

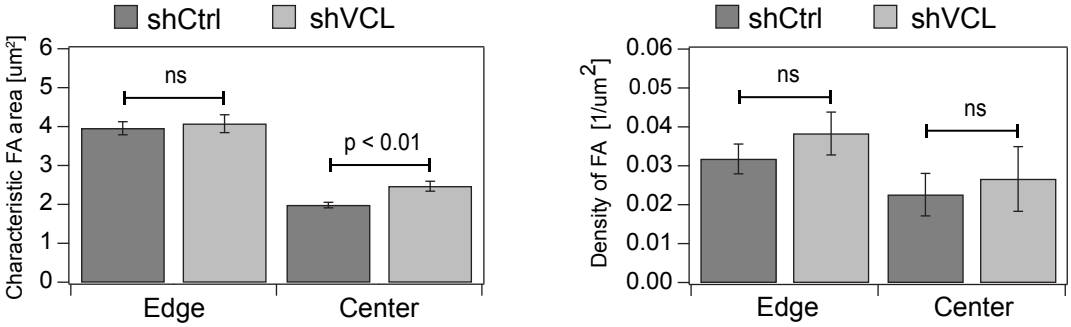

Stubb, Guzmán et al. Supplementary Figure 6

a.

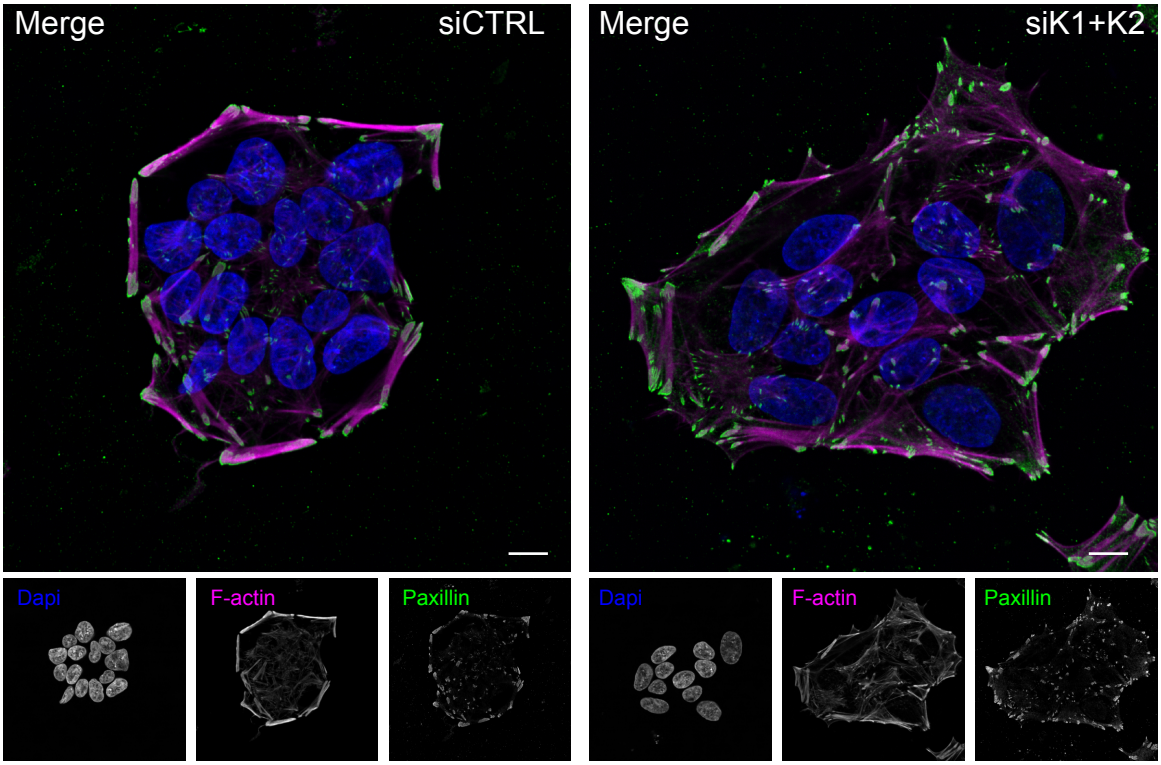

b.

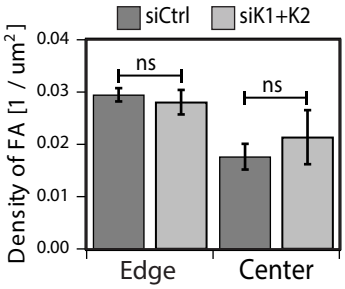

Stubb, Guzmán et al. Supplementary Figure 7